Long-term trends in urban NO2 concentrations and associated pediatric asthma cases: estimates from global datasets

Susan Anenberg[1,1], Arash Mohegh[1,1], Daniel L. Goldberg[2,2], Michael Brauer[3,3], Katrin Burkart[4,4], Perry Hystad[5,5], Andrew Larkin[5,5], and Sarah Wozniak[4,4]

[1]George Washington University
[2]George Washington University,Argonne National Laboratory
[3]University of British Columbia,Institute for Health Metrics and Evaluation
[4]Institute for Health Metrics and Evaluation
[5]Oregon State University

November 30, 2022

Abstract

Background: Combustion-related nitrogen dioxide (NO2) air pollution is associated with pediatric asthma incidence. We estimated global surface NO2 concentrations consistent with the Global Burden of Disease Study for 1990-2019 at 1km resolution, and concentrations and attributable pediatric asthma incidence trends in 13,189 cities from 2000-2019. Methods: We scaled an existing surface annual average NO2 concentrations dataset for 2010-2012 from a land use regression model (based on 5,220 NO2 monitors in 58 countries and land use variables) to other years using NO2 column densities from satellite and reanalysis datasets. We applied these concentrations to epidemiologically-derived concentration-response factors, population, and baseline asthma rates to estimate NO2-attributable pediatric asthma incidence. Findings: We estimated that 1.85 million (95% uncertainty interval: 0.93 – 2.8 million) new pediatric asthma cases were attributable to NO2 globally in 2019, two-thirds of which occurred in urban areas. The fraction of pediatric asthma incidence that is attributable to NO2 in urban areas declined from 20% in 2000 to 16% in 2019. Urban attributable fractions dropped in High-income (-41%), Latin America/Caribbean (-16%), Central Europe, Eastern Europe, and Central Asia (-13%), and Southeast Asia, East Asia, and Oceania (-6%), and rose in South Asia (+23%), Sub-Saharan Africa (+11%), and North Africa and Middle East (+5%) regions. The importance of NO2 concentrations, pediatric population size, and asthma incidence rates in driving these changes differs regionally. Interpretation: Despite improvements in some regions, combustion-related NO2 pollution continues to be an important contributor to pediatric asthma incidence globally, particularly in cities. Funding: Health Effects Institute, NASA

Long-term trends in urban NO_2 concentrations and associated pediatric asthma incidence: estimates from global datasets

Susan C. Anenberg[1*], Arash Mohegh[1*], Daniel L. Goldberg[1,2], Gaige H. Kerr[1], Michael Brauer[3,4], Katrin Burkart[3], Perry Hystad[5], Andrew Larkin[5], Sarah Wozniak[3], Lok Lamsal[6]

1 Milken Institute School of Public Health, George Washington University, Washington, DC, USA

2 Energy Systems Division, Argonne National Laboratory, Washington, DC, USA

3 Institute for Health Metrics and Evaluation, University of Washington, Seattle, Washington, USA

4 University of British Columbia, Vancouver, BC, Canada

5 Oregon State University, Corvallis, OR, USA

6 NASA Goddard Space Flight Center, Greenbelt, MD, USA

* These authors contributed equally to this work.

Corresponding author: Susan Anenberg, 950 New Hampshire Ave NW, Washington, DC 20052, sanenberg@gwu.edu, 1-202-994-2392

Abstract

Background: Combustion-related nitrogen dioxide (NO_2) air pollution is associated with pediatric asthma incidence. We estimated global surface NO_2 concentrations consistent with the Global Burden of Disease Study for 1990-2019 at 1km resolution, and concentrations and attributable pediatric asthma incidence trends in 13,189 cities from 2000-2019.

Methods: We scaled an existing surface annual average NO_2 concentrations dataset for 2010-2012 from a land use regression model (based on 5,220 NO_2 monitors in 58 countries and land use variables) to other years using NO_2 column densities from satellite and reanalysis datasets. We applied these concentrations to epidemiologically-derived concentration-response factors, population, and baseline asthma rates to estimate NO_2-attributable pediatric asthma incidence.

Findings: We estimated that 1.85 million (95% uncertainty interval: 0.93 – 2.8 million) new pediatric asthma cases were attributable to NO_2 globally in 2019, two-thirds of which occurred in urban areas. The fraction of pediatric asthma incidence that is attributable to NO_2 in urban areas declined from 20% in 2000 to 16% in 2019. Urban attributable fractions dropped in High-income (-41%), Latin America/Caribbean (-16%), Central Europe, Eastern Europe, and Central Asia (-13%), and Southeast Asia, East Asia, and Oceania (-6%), and rose in South Asia (+23%), Sub-Saharan Africa (+11%), and North Africa and Middle East (+5%) regions. The importance of NO_2 concentrations, pediatric population size, and asthma incidence rates in driving these changes differs regionally.

Interpretation: Despite improvements in some regions, combustion-related NO_2 pollution continues to be an important contributor to pediatric asthma incidence globally, particularly in cities.

Funding: Health Effects Institute, NASA

Research in context:

Evidence before this study: We searched PubMed and Google Scholar databases for studies published in English from the database inception until March 11, 2021, using the search terms ("NO_2" OR "nitrogen dioxide") AND "asthma" AND "trends". Previous studies have reported epidemiological analyses linking changes with asthma to changes in NO_2, or have assessed long-term trends in NO_2 concentrations in some countries or world regions. However, these studies provide little information about how NO_2 concentrations are changing in urban areas all around the world, and the influence those changes have on pediatric asthma incidence. An earlier study published in 2019 showed that over 4 million new pediatric asthma cases, representing ~13% of all pediatric asthma incidence worldwide in 2015, could be attributed to NO_2 pollution. Understanding temporal trends in NO_2-attributable pediatric asthma incidence could help inform asthma and air pollution mitigation strategies.

Added value of this study: We show that urban areas experience higher NO_2 concentrations and disease burdens compared with rural areas, with 16% of pediatric asthma incidence in urban areas estimated to be attributable to NO_2 pollution. We also find that the fraction of pediatric asthma incidence that is attributable to NO_2 declined in High-income, Latin American and Caribbean, Central Europe, Eastern Europe, and Central Asia from 2000 to 2019, and increased in the rest of the world, particularly in South Asia and Sub-Saharan Africa. In carrying out this work, we produced the most spatially resolved (1km x 1km) long-term (1990-2019) dataset of surface NO_2 concentrations, which is compatible with the Global Burden of Disease Study and is now publicly available. Our study also demonstrates the utility of satellite remote sensing for environmental and public health surveillance in urban areas worldwide.

Implications of all the available evidence: Current levels of NO_2 contribute substantially to pediatric asthma incidence, particularly in cities. Mitigating air pollution should be a critical element of children's public health strategies.

Acknowledgements: This work was supported by grants from the Health Effects Institute/Bloomberg Philanthropies (Research Agreement #4977/20-11) and NASA (Grant #80NSSC19K0193). We gratefully acknowledge the developers of the OMI NO_2 concentration products, GHS-SMOD urban area dataset, GBD disease rate datasets, and Worldpop population dataset. We appreciate helpful discussions with Bryan Duncan. The contents of this article do not necessarily reflect the views of HEI, or its sponsors.

Data availability: NO_2 concentrations are available at: https://figshare.com/articles/dataset/Global_surface_NO2_concentrations_1990-2020/12968114.

Estimated NO_2-attributable asthma incidence results are available at: https://github.com/AMohegh/Asthma_NO2_urban

Author contributions: SCA, AM, and DG designed the study; PH, AL, and LL provided data; AM and GK carried out the calculations, SCA, AM, DG, MB, PH, AL, and SW contributed input on methods development; SCA and AM wrote the paper; all authors helped interpret results and reviewed the manuscript. AM, GK, and DG have verified the underlying data.

Declaration of interests: The authors declare no conflict of interest.

Introduction

Nitrogen dioxide (NO_2), a component of nitrogen oxides (NO_x), is a pervasive air pollutant that is a precursor for ground-level ozone and fine particulate matter ($PM_{2.5}$), the leading contributors to air pollution-related mortality.[1] Major anthropogenic NO_2 sources include on-road and non-road transportation tailpipe emissions (including heavy-, medium-, and light-duty vehicles, shipping, and aviation), power plants, industrial manufacturing, and agriculture.[2–5] NO_2 is an effective tracer for anthropogenic fuel combustion generally, and traffic specifically, especially in urban areas.[6–9] NO_2 concentration trends can be used to evaluate the efficacy of air pollution regulations, as well as effects of abrupt emission changes (e.g. power plant closures, new oil and gas fields, COVID-19 lockdowns).[10–14]

Beyond its role in $PM_{2.5}$ and ozone formation, NO_2 itself has been associated with adverse health outcomes including asthma exacerbation.[15,16] Epidemiological studies have also found associations between transportation-related air pollutants with new onset asthma in children.[17,18] While the putative agent in the traffic-related air pollution mixture remains unknown, epidemiological studies are relatively consistent in their finding that NO_2 is significantly associated with pediatric asthma incidence, while the evidence for other traffic-related air pollutants (e.g. $PM_{2.5}$) is more mixed.[17,18] Previous health impact assessments have linked NO_2 with ~13% of the global pediatric asthma burden, and up to ~50% in the most populated 250 cities worldwide.[19,20]

NO_x emissions and NO_2 concentrations have changed dramatically in response to socioeconomic changes and regulation, even prior to the large-scale activity changes during the COVID-19 pandemic.[21–25] In the U.S., average NO_2 concentrations dropped ~50% from the 1980s to 2010s,[26] with larger drops near major roadways[26] and point sources.[10] In the last two decades, U.S. NO_x emissions fell ~3-6% per year as vehicles got more fuel efficient and cleaner and power plants shifted from coal to relatively cleaner fuels (e.g. natural gas).[11,27,28] NO_2 concentrations have also decreased in Europe, though more slowly.[29,30] In contrast, NO_2 has increased in India,[31] the Middle East,[32] and Eastern Europe.[23] In China, NO_x emissions peaked around 2011/2012 and subsequently declined.[33–35]

NO_2 pollution is a pediatric health challenge in cities, driven by higher population growth, particularly in Asia and Africa where NO_2 concentrations have risen since 2000, and higher asthma rates in cities compared with national averages. Previous research on NO_2 temporal trends have focused on small subsets of cities and have not considered its health impacts, precluding globally consistent comparisons of trends in NO_2 concentrations and associated health burdens. The global coverage and long continuous record of satellite remote sensing since the 1990s makes it possible to track NO_2 concentrations globally.[36–39] Additionally, the high spatial resolution of current satellites can capture NO_2 variation at urban and intra-urban scales.[40,41]

Here we investigate long-term trends of annual average NO_2 concentrations and associated pediatric asthma burdens in 13,189 urban areas over the past two decades globally. We first generate a new gridded global surface annual average NO_2 concentration dataset from 1990 to 2019 that is compatible with the spatiotemporal coverage of the Global Burden of Disease (GBD) Study. We then explore trends in NO_2 concentrations and attributable pediatric asthma incidence for urban areas from 2000 to 2019, for which estimated concentrations have greater certainty due to available ground monitoring. Finally, we deconstruct the drivers of these trends to explore the influence of NO_2 concentrations versus demographic changes.

Methods

We integrated global environmental and demographic datasets from different sources to generate new estimates of surface NO_2 concentrations globally and NO_2-attributable pediatric asthma incidence in cities. The analysis was done in Python (version 3.6.7).

Globally gridded NO_2 *concentrations*

We generated a new dataset of surface annual average NO_2 concentrations at 0.0083° (~1 km^2) resolution in five-year increments from 1990-2010 and annually from 2010-2019, consistent with the GBD 2020 analysis years. We used an existing global NO_2 concentration dataset (2010-2012 average) at 100m resolution from a land use regression (LUR) model described by Larkin et al.[8,42] and made adjustments to correct for a high bias in rural areas and to scale concentrations to additional years (Figure S1). A full description of the methods and data sources used to construct the concentration dataset is in the Supplemental Material.

For the base year 2011, we used the Larkin et al.[42] LUR estimates directly in all gridcells categorized as "urban" according to the Global Human Settlement Model grid[43] or that include major roadways. The LUR used annual measurements from 5,220 air monitors in 58 countries (mostly in Europe, North America, and Asia) with inputs from road networks and other land use variables and satellite NO_2 column observations. Globally, the model captured 54% of NO_2 variation, with a mean absolute error of 3.7 ppb. Model performance differed regionally: R^2 varied from 0.42 in Africa to 0.67 in South America. In North America, Europe, and Asia, R^2 (0.52 for each region) approximately matched the global average (0.54). For rural areas, we found that the Larkin et al.[42] dataset was biased high, and therefore adjusted concentrations using surface NO_2 concentrations derived from Ozone Monitoring Instrument (OMI) satellite NO_2 columns (Figure S2). After adjusting the 2011 rural NO_2 concentration estimates, we scaled all 2011 gridcell concentrations to the GBD 2020 analysis period (1990-2019) using the MERRA-2 reanalysis product[44] for 1990, 1995, and 2000 and OMI NO_2 column densities for 2005-2019 (Figure S3).

As Larkin et al.[42] demonstrated that their NO_2 concentrations agreed well with urban ground observations, we added evaluations of the changes made in this work: 1) we compared our 2011 rural NO_2 concentration estimates to the European Monitoring and Evaluation Program (EMEP) ground monitoring dataset, which has a large number of stations in rural areas, while “rural” monitors in other ground monitoring networks are often located directly downwind from urban areas; 2) we compared our 2019 concentrations in urban and rural areas against 4,348 monitors in the U.S., Canada, and Europe.

While we created this spatially (all urban and rural areas globally) and temporally complete (1990-2019) concentration dataset for compatibility with the GBD 2020, we focused our trend analysis on urban areas over the last two decades (2000-2019), for which estimated concentrations have greater certainty due to available ground monitoring.

NO_2*-attributable pediatric asthma incidence*

We estimated NO_2-attributable cases of pediatric asthma incidence using an epidemiologically-derived concentration response function, following previous studies[19,20] (Equation 1):

Equation 1:
$$Burden_{k,\mathrm{a}} = \sum_{Grid\ cells\ in\ \mathrm{k}} Inc_{c,\mathrm{a}} \times Pop_{i,j,\mathrm{a}} \times (1 - e^{-\beta X_{i,j}})$$

where *Burden* is the NO_2-attributable asthma incidence in city *k* for age group *a*, *Inc* is the baseline asthma incidence rate for age group *a* and country *c*, *Pop* is the population in gridcell *i,j* for age group *a*, β is the concentration response factor relating the NO_2 concentration with increased risk of pediatric asthma incidence, and *X* is the annual average NO_2 concentration in gridcell *i,j*. We regridded all datasets to 1km resolution and estimated NO_2-attributable asthma incidence in each gridcell. We previously found that this resolution balances accuracy with computational efficiency in estimating city-level NO_2-attributable disease burdens.[20] We sum results across all gridcells within each city for a city-level total.

We applied a relative risk (RR) of 1.26 [95% uncertainty interval (UI): 1.1 – 1.37] per 10 ppb annual average NO_2 concentration increase from a large epidemiological meta-analysis, and calculated uncertainty in NO_2-attributable pediatric asthma incidence using the statistical error in this RR estimate.[17] As RR error is static over time it does not influence temporal trends. We used a low concentration threshold of 2 ppb annual average NO_2 concentration, the 5th percentile of the minimum concentrations reported by the studies in the meta-analysis. Alternative low-concentration thresholds would not substantially affect estimated trends in NO_2-attributable asthma incidence, since thresholds are applied uniformly across gridcells and only 3% of year-specific urban concentrations were below 2 ppb.

We used population estimates from Worldpop[45] from 2000-2019 for ages 1-4, 5-9, 10-14, and 15-18 years old at ~1km resolution, and summed results across age groups for total NO_2-attributable pediatric asthma incidence. National baseline annual asthma incidence rates from

2000-2019 were from the GBD 2019 Study. Urban area boundaries were from the GHS-SMOD Urban Centre dataset for 2015 (latest year, applied here to all years).[43] We consider gridcells and *in-situ* monitors (used to evaluate the concentration dataset) to be part of an "urban cluster" if they are located in "urban" and "suburban" areas in the GHS-SMOD dataset, defined as areas with >300 people per km^2 that are part of clusters with >5,000 people. All other gridcells and monitors are considered "rural". World regions definitions are from the GBD 2019 Study (Table S2 and Figure S4).[1]

Drivers of change

To disentangle the drivers of temporal trends in NO_2-attributable pediatric asthma incidence, we isolated the contribution of exposure, population size, and baseline asthma rates using: 1) the core results with annually varying data inputs, and 2) three sets of simulations in which we revert one contributing parameter back to 2000 (see Supplemental Material for more details). Cohen et al.[46] used a similar approach for disentangling drivers of national $PM_{2.5}$ disease burdens. We ignored interactions between the contributing factors (e.g. the influence of changing NO_2 concentrations on baseline asthma rates), as we considered them to be minor relative to many other influences on these multi-factorial parameters (e.g. the effects of health care advances on baseline asthma rates).

Role of the funding source

The funders of the study had no role in study design, data collection, data analysis, data interpretation, or writing of the report. SA and AM had full access to all the data in the study and had final responsibility for the decision to submit for publication.

Results

Our new NO_2 concentration dataset reduces the 2010-2012 Larkin et al.[42] rural high concentrations bias [mean bias (MB) reduced from 2.4 to 1.0 ppb; Table S1 and Figure S6] and captures observed surface-level concentrations in both urban and rural areas in 2019 (MB = 3.3, 1.7, and 2.3 in Canada, U.S., and Europe, respectively; Figure S7). See the Supplemental Material for further evaluation description and results. Estimated NO_2 concentrations are highest in the most populated regions of the world, including North America, Europe, and South and East Asia throughout the time period (Figure 1). Cities with the 10 highest NO_2 concentrations in 2019 were located in the Middle East (Lebanon, Iraq, Iran), China, and Russia (Figure S8).

We estimated that the global population-weighted average annual mean NO_2 concentration was 6.6 ppb in 2019, leading to 1.85 million (95% UI: 0.93 – 2.8 million) new asthma cases among children worldwide that year, or 8.5% (95% UI: 4.3% – 12.8%) of all pediatric asthma incidence (Figure 2). Approximately two-thirds of NO_2-attributable pediatric asthma incidence occurred in the 13,189 urban areas (1.22 million cases; 95% UI: 0.60 – 1.8 million). Compared with rural areas, urban areas had 2-4 times higher population-weighted NO_2 concentrations (10.6 ppb in urban areas versus 4.2 ppb in rural areas), NO_2-attributable asthma cases (1.22 million versus

0.63 million), NO_2-attributable asthma cases per 100,000 (156 versus 40), and attributable fractions (16.4% versus 4.5%) in 2019.

Focusing on urban areas in the last two decades, we found that annual average NO_2 concentrations decreased by 13%, from 12.2 ppb in 2000 to 10.6 ppb in 2019, with a steady decline from 2011 to 2019 after rising from 2000 to 2011 (Figure 2). NO_2 concentrations in High-income cities exceeded the global average throughout the time period, despite declining 38% from 17.6 ppb in 2000 to 11.0 ppb in 2019 (Figure 3). Contrastingly, concentrations in South Asia and Sub-Saharan Africa rose by 18% (8.6 to 10.1 ppb) and 11% (6.4 to 7.1 ppb), respectively, but remained lower than the global urban average throughout the time period. These large regional groupings of cities obscure contrasting trends between sub-regions in some cases (Figure S9).

We estimated that ~1.2 million pediatric asthma cases in urban areas globally were attributable to NO_2 pollution in both 2000 and 2019, though the rate per 100,000 children declined 14% from 176 to 156 per 100,000 children as the urban pediatric population grew by 12% (Figure 2). High-income cities had the most NO_2-attributable asthma incidence in 2019, with 341,000 cases or 28% of the global urban total, despite having only 14% of the global urban pediatric population (Figure 4 and Table S4). While total NO_2-attributable pediatric asthma cases were in the most populated cities of the world (Figure S10), all 10 highest attributable rates were in the U.S. (Figure S11). Contrastingly, cities in South Asia, with approximately a quarter of the global pediatric population, only accounted for 7% of global urban NO_2-attributable pediatric asthma incidence. NO_2-attributable pediatric asthma incidence rates were also highest in the High-income region (311 attributable cases per 100,000 children) and were an order of magnitude lower in South Asia (50).

The fraction of pediatric asthma incidence that was estimated to be attributable to NO_2 across all 13,189 urban areas globally dropped from 19.7% in 2000 to 16.4% in 2019 (Figure 2). Urban attributable fractions dropped between 2000 and 2019 in High-income (-41%), Latin America and Caribbean (-16%), Central Europe, Eastern Europe, and Central Asia (-13%), and Southeast Asia, East Asia, and Oceania (-6%) regions, and rose in South Asia (+23%), Sub-Saharan Africa (+11%), and North Africa and Middle East (+5%) regions. The large decrease in High-income cities is partly driven by even larger drops in North America (-52%; Figure S8). The 35% increase in Central Europe, Eastern Europe, and Central Asia was driven by >50% increases in Central Asia and Eastern Europe, balanced by a 14% decrease in Central Europe. In 2019, regional urban average attributable fractions ranged from 10% in Sub-Saharan Africa to 20% in Central Europe, Eastern Europe, and Central Asia and North Africa and Middle East. As for concentrations, the 10 highest attributable fractions were located in Lebanon, Iraq, Iran, China, and Russia (Figure S11).

Estimated temporal trends in urban NO_2-attributable pediatric asthma incidence are driven by simultaneous and often competing changes in NO_2 concentrations, pediatric population, and asthma incidence rates (Figure 5). Australasia and High-income Asia Pacific are the only regions where declining concentrations, pediatric population size, and asthma rates all contribute to overall drops in NO_2-attributable pediatric asthma incidence. The opposite occurred in Central, South, and Southeast Asia, and in North Africa and the Middle East, where concentrations, pediatric population, and asthma rates all rose. In High-income North America, Western Europe, and several other regions, declining NO_2 concentrations were offset by increases in asthma incidence rates and/or pediatric population size. These competing influences changed over time, with declining concentrations becoming more influential over time in North America and Southern Latin America, and population growth becoming more influential in North Africa and Middle East and Southern Sub-Saharan Africa (Figure S12).

Discussion

We estimated that 1.84 million (95% UI: 0.93 – 2.8 million) pediatric asthma cases globally could be attributable to NO_2 pollution in 2019. Despite having only one-third of the global pediatric population, urban areas had two-thirds of NO_2-attributable pediatric asthma incidence. The NO_2-attributable fraction of pediatric asthma incidence in urban areas globally declined from 20% in 2000 to 16% in 2019. Regional trends were inconsistent: urban average attributable fractions dropped in High-income cities; Latin America and Caribbean; Central Europe, Eastern Europe, and Central Asia; and Southeast Asia, East Asia, and Oceania, and rose in South Asia; Sub-Saharan Africa; and North Africa and Middle East. The drivers of temporal trends in NO_2 concentrations and pediatric asthma burdens were also inconsistent regionally, with declining NO_2 concentrations in some regions counteracted by increases in pediatric population size and asthma incidence rates.

Our study is consistent with the broader literature demonstrating that NO_2 is largely an urban pollutant.[7,47–49] Estimated NO_2 concentration trends are consistent with recent studies using satellite data to investigate NO_2 concentration trends during 2004-2018 for the U.S., Europe, China, India, and Japan.[23,31,50] For example, Qu et al.[51] also showed a similar decrease in U.S. NO_2 concentrations based on ground observations, satellite data, and modeling outputs from 2006-2016, and Henneman et al.[26] showed a similar decrease using ground observations from 1980-2020. A recent study focused on biomass burning in the equatorial Africa region found declining concentrations from 2005 to 2017[52], while we found an increase in Sub-Saharan Africa from 2000-2019. A biomass burning decline in the region may be smaller and offset by anthropogenic emission changes in populated urban areas.

While our new NO_2 dataset leverages advantages of different data sources, concentrations remain uncertain. Many cities, particularly in low- and middle-income countries (LMICs), still lack ground NO_2 monitors, challenging calibration and evaluation of LUR models.[42] Urban NO_2 concentrations are therefore more certain in North America, Europe, and Asia, compared with Africa and South America. Rural concentrations are uncertain globally with limited ground monitoring outside of urban areas. Scaling the 2010-2012 LUR NO_2 concentrations to other years assumes that the land use predictors are static over time. This assumption is likely supported by slow changes in road density and volume and urban form, but over the two decades explored here, some land use evolution is likely[53], particularly in rapidly developing LMICs. The directional impact of these uncertainties on results is unknown.

Our estimate of the global burden of NO_2 on pediatric asthma incidence in 2019 is less than half of the 4.2 million found by Achakulwisut et al.[19] for 2015. Our results for India are also lower than previous estimates while our U.S. results are higher.[17,20] Several factors explain this discrepancy. First, our new NO_2 concentrations correct for a high rural NO_2 bias, leading to lower NO_2-attributable asthma incidence estimates, especially in countries with larger rural populations (e.g. India). Second, GBD 2019 baseline asthma rates are much lower than in previous versions, except in high income areas (e.g. U.S.), due to a change in the case definition used which lowered estimated rates in most places and raised them for the U.S.[54] For example, baseline pediatric asthma incidence rates in 2015 (the year analyzed by Mohegh et al.[20]) in the GBD 2019 were 81% of GBD 2017 values. Contrastingly, U.S. pediatric asthma incidence rates were a factor of 2.2 higher in the GBD 2019 versus GBD 2017. Changes in baseline asthma rates approximately proportionally affect estimated NO_2-attributable pediatric asthma incidence. Our NO_2 attributable fraction result in High-Income North America in 2019 (17.3%) was similar to a previous estimate for the U.S. in 2000 (17.9%), though our NO_2 concentrations were lower (10.9 ppb in urban areas vs. 13.2 ppb overall).[47] The different analysis years are important since, as we have shown, NO_2 concentrations trends are changing rapidly.

The health impact assessment method also introduces uncertainties. While we used national pediatric asthma rates, asthma prevalence varies within countries.[47] Living in urban areas has been associated with increased risk of asthma prevalence in LMICs[55] and asthma-related emergency department visits and hospitalizations in the U.S.[56] Similarly, temporal trends in baseline asthma incidence may differ in urban areas compared with national averages, especially in rapidly urbanizing LMICs. If asthma prevalence is higher in urban areas compared with national averages, NO_2-attributable asthma incidence may be underestimated. In addition, it is currently unknown whether pediatric asthma incidence is associated with NO_2, the traffic-related air pollution mixture, or the broader combustion-related air pollution mixture. Finally, the 1km resolution of our NO_2 concentration estimates may not capture areas with co-located steep spatial gradients in concentrations and population, potentially leading NO_2-attributable asthma incidence to be underestimated.

Despite these uncertainties and limitations, our results demonstrate the important influence of combustion-related air pollution on children's health in cities globally. In places that have effective air quality management programs (e.g. U.S., Europe), NO_2 concentrations have been trending downward for decades, with benefits for children's respiratory health. Even with these improvements, current NO_2 levels contribute substantially to pediatric asthma incidence, highlighting that mitigating air pollution should be a critical element of children's public health strategies. For cities that have not benefited from strong local or national-scale air quality management programs, the experience of cities that have such programs demonstrates that addressing combustion-related air pollution can lead to major air quality and public health improvements over relatively short time frames (years). These air quality improvements can be achieved through either end-of-pipe emission control technologies such as catalytic converters or avoiding the combustion in the first place, which would have additional benefits from reduced greenhouse gas emissions.

Our study demonstrates the value of satellite remote sensing and statistical models for tracking NO_2 pollution and for environmental health surveillance at local, national, and global scales. The combination of methods offers strengths beyond the capabilities of each technique alone: a long and consistent observational record of NO_2 column densities from satellites with the high spatial resolution of surface concentration predictions from LUR models. Future studies may leverage these data sources and others, including new satellite sensors that have higher temporal and spatial resolutions, mobile monitoring, distributed ground sensor networks, and chemical transport models, to further improve the accuracy and spatiotemporal resolution of NO_2 concentration estimates. Further, our study shows the importance of considering demographic changes over time for understanding air pollution health risks. Improved and more widely accessible information about disease rates, and capturing population distribution and movement, will enable more accurate and highly resolved air pollution health impact assessments.

References

(1) GBD 2019 Risk Factor Collaborators. Global Burden of 87 Risk Factors in 204 Countries and Territories, 1990–2019: A Systematic Analysis for the Global Burden of Disease Study 2019. *The Lancet* **2020**, *396* (10258), 1223–1249. https://doi.org/10.1016/S0140-6736(20)30752-2.

(2) McDuffie, E. E.; Smith, S. J.; O'Rourke, P.; Tibrewal, K.; Venkataraman, C.; Marais, E. A.; Zheng, B.; Crippa, M.; Brauer, M.; Martin, R. V. A Global Anthropogenic Emission Inventory of Atmospheric Pollutants from Sector- and Fuel-Specific Sources (1970–2017): An Application of the Community Emissions Data System (CEDS). *Earth Syst. Sci. Data* **2020**, *12* (4), 3413–3442. https://doi.org/10.5194/essd-12-3413-2020.

(3) Anenberg, S.; Miller, J.; Minjares, R.; Du, L.; Henze, D. K.; Lacey, F.; Malley, C. S.; Emberson, L.; Franco, V.; Klimont, Z.; Heyes, C. Impacts and Mitigation of Excess Diesel-Related NOx Emissions in 11 Major Vehicle Markets. *Nature* **2017**, *545*, 467–471. https://doi.org/10.1038/nature22086.

(4) Stohl, A.; Aamaas, B.; Amann, M.; Baker, L. H.; Bellouin, N.; Berntsen, T. K.; Boucher, O.; Cherian, R.; Collins, W.; Daskalakis, N.; Dusinska, M.; Eckhardt, S.; Fuglestvedt, J. S.; Harju, M.; Heyes, C.; Hodnebrog, ø.; Hao, J.; Im, U.; Kanakidou, M.; Klimont, Z.; Kupiainen, K.; Law, K. S.; Lund, M. T.; Maas, R.; MacIntosh, C. R.; Myhre, G.; Myriokefalitakis, S.; Olivié, D.; Quaas, J.; Quennehen, B.; Raut, J.-C.; Rumbold, S. T.; Samset, B. H.; Schulz, M.; Seland, ø.; Shine, K. P.; Skeie, R. B.; Wang, S.; Yttri, K. E.; Zhu, T. Evaluating the Climate and Air Quality Impacts of Short-Lived Pollutants. *Atmospheric Chem. Phys.* **2015**, *15* (18), 10529–10566. https://doi.org/10.5194/acp-15-10529-2015.

(5) Crippa, M.; Guizzardi, D.; Muntean, M.; Schaaf, E.; Dentener, F.; van Aardenne, J. A.; Monni, S.; Doering, U.; Olivier, J. G. J.; Pagliari, V.; Janssens-Maenhout, G. Gridded Emissions of Air Pollutants for the Period 1970–2012 within EDGAR v4.3.2. *Earth Syst. Sci. Data* **2018**, *10* (4), 1987–2013. https://doi.org/10.5194/essd-10-1987-2018.

(6) Stavrakou, T.; Müller, J.-F.; Boersma, K. F.; De Smedt, I.; van der A, R. J. Assessing the Distribution and Growth Rates of NOx Emission Sources by Inverting a 10-Year Record of NOx Satellite Columns. *Geophys. Res. Lett.* **2008**, *35* (10). https://doi.org/10.1029/2008GL033521.

(7) Bechle, M. J.; Millet, D. B.; Marshall, J. D. Effects of Income and Urban Form on Urban NO2: Global Evidence from Satellites. *Environ. Sci. Technol.* **2011**, *45* (11), 4914–4919. https://doi.org/10.1021/es103866b.

(8) Geddes, J. A.; Martin, R. V.; Boys, B. L.; van Donkelaar, A. Long-Term Trends Worldwide in Ambient NO2 Concentrations Inferred from Satellite Observations. *Environ. Health Perspect.* **2016**, *124* (3), 281–289. https://doi.org/10.1289/ehp.1409567.

(9) Bechle, M. J.; Millet, D. B.; Marshall, J. D. Does Urban Form Affect Urban NO2? Satellite-Based Evidence for More than 1200 Cities. *Environ. Sci. Technol.* **2017**, *51* (21), 12707–12716. https://doi.org/10.1021/acs.est.7b01194.

(10) Duncan, B. N.; Yoshida, Y.; de Foy, B.; Lamsal, L. N.; Streets, D. G.; Lu, Z.; Pickering, K. E.; Krotkov, N. A. The Observed Response of Ozone Monitoring Instrument (OMI) NO2 Columns to NOx Emission Controls on Power Plants in the United States: 2005–2011. *Atmos. Environ.* **2013**, *81*, 102–111. https://doi.org/10.1016/j.atmosenv.2013.08.068.

(11) Silvern, R. F.; Jacob, D. J.; Mickley, L. J.; Sulprizio, M. P.; Travis, K. R.; Marais, E. A.; Cohen, R. C.; Laughner, J. L.; Choi, S.; Joiner, J.; Lamsal, L. N. Using Satellite

Observations of Tropospheric NO2 Columns to Infer Long-Term Trends in US NOx Emissions: The Importance of Accounting for the Free Tropospheric NO2 Background. *Atmospheric Chem. Phys.* **2019**, *19* (13), 8863–8878. https://doi.org/10.5194/acp-19-8863-2019.

(12) Dix, B.; Bruin, J.; Roosenbrand, E.; Vlemmix, T.; Francoeur, C.; Gorchov-Negron, A.; McDonald, B.; Zhizhin, M.; Elvidge, C.; Veefkind, P.; Levelt, P.; Gouw, J. Nitrogen Oxide Emissions from U.S. Oil and Gas Production: Recent Trends and Source Attribution. *Geophys. Res. Lett.* **2020**, *47* (1). https://doi.org/10.1029/2019GL085866.

(13) Goldberg, D. L.; Anenberg, S. C.; Griffin, D.; McLinden, C. A.; Lu, Z.; Streets, D. G. Disentangling the Impact of the COVID-19 Lockdowns on Urban NO_2 From Natural Variability. *Geophys. Res. Lett.* **2020**, *47* (17). https://doi.org/10.1029/2020GL089269.

(14) Kerr, G. H.; Goldberg, D. L.; Anenberg, S. C. COVID-19 Pandemic Reveals Persistent Disparities in Nitrogen Dioxide Pollution. *Proc. Natl. Acad. Sci.* **2021**, *In press*.

(15) Perez, L.; Lurmann, F.; Wilson, J.; Pastor, M.; Brandt, S. J.; Künzli, N.; McConnell, R. Near-Roadway Pollution and Childhood Asthma: Implications for Developing "Win–Win" Compact Urban Development and Clean Vehicle Strategies. *Environ. Health Perspect.* **2012**, *120* (11), 1619–1626. https://doi.org/10.1289/ehp.1104785.

(16) Gauderman, W. J.; Avol, E.; Lurmann, F.; Kuenzli, N.; Gilliland, F.; Peters, J.; McConnell, R. Childhood Asthma and Exposure to Traffic and Nitrogen Dioxide: *Epidemiology* **2005**, *16* (6), 737–743. https://doi.org/10.1097/01.ede.0000181308.51440.75.

(17) Khreis, H.; Kelly, C.; Tate, J.; Parslow, R.; Lucas, K.; Nieuwenhuijsen, M. Exposure to Traffic-Related Air Pollution and Risk of Development of Childhood Asthma: A Systematic Review and Meta-Analysis. *Environ. Int.* **2017**, *100*, 1–31. https://doi.org/10.1016/j.envint.2016.11.012.

(18) Anenberg, S. C.; Henze, D. K.; Tinney, V.; Kinney, P. L.; Raich, W.; Fann, N.; Malley, C. S.; Roman, H.; Lamsal, L.; Duncan, B.; Martin, R. V.; van Donkelaar, A.; Brauer, M.; Doherty, R.; Jonson, J. E.; Davila, Y.; Sudo, K.; Kuylenstierna, J. C. I. Estimates of the Global Burden of Ambient PM2.5, Ozone, and NO2 on Asthma Incidence and Emergency Room Visits. *Environ. Health Perspect.* **2018**, *126* (10), 107004. https://doi.org/10.1289/EHP3766.

(19) Achakulwisut, P.; Brauer, M.; Hystad, P.; Anenberg, S. C. Global, National, and Urban Burdens of Paediatric Asthma Incidence Attributable to Ambient NO2 Pollution: Estimates from Global Datasets. *Lancet Planet. Health* **2019**, *3* (4), e166–e178. https://doi.org/10.1016/S2542-5196(19)30046-4.

(20) Mohegh, A.; Goldberg, D.; Achakulwisut, P.; Anenberg, S. C. Sensitivity of Estimated NO2-Attributable Pediatric Asthma Incidence to Grid Resolution and Urbanicity. *Environ. Res. Lett.* **2020**, *16* (1), 014019. https://doi.org/10.1088/1748-9326/abce25.

(21) Lamsal, L. N.; Duncan, B. N.; Yoshida, Y.; Krotkov, N. A.; Pickering, K. E.; Streets, D. G.; Lu, Z. U.S. NO2 Trends (2005–2013): EPA Air Quality System (AQS) Data versus Improved Observations from the Ozone Monitoring Instrument (OMI). *Atmos. Environ.* **2015**, *110*, 130–143. https://doi.org/10.1016/j.atmosenv.2015.03.055.

(22) Miyazaki, K.; Eskes, H.; Sudo, K.; Boersma, K. F.; Bowman, K.; Kanaya, Y. Decadal Changes in Global Surface NOx Emissions from Multi-Constituent Satellite Data Assimilation. *Atmospheric Chem. Phys.* **2017**, *17* (2), 807–837. https://doi.org/10.5194/acp-17-807-2017.

(23) Georgoulias, A. K.; van der A, R. J.; Stammes, P.; Boersma, K. F.; Eskes, H. J. Trends and Trend Reversal Detection in 2 Decades of Tropospheric NO2 Satellite Observations. *Atmospheric Chem. Phys.* **2019**, *19* (9), 6269–6294. https://doi.org/10.5194/acp-19-6269-2019.
(24) Tong, D. Q.; Lamsal, L.; Pan, L.; Ding, C.; Kim, H.; Lee, P.; Chai, T.; Pickering, K. E.; Stajner, I. Long-Term NOx Trends over Large Cities in the United States during the Great Recession: Comparison of Satellite Retrievals, Ground Observations, and Emission Inventories. *Atmos. Environ.* **2015**, *107*, 70–84. https://doi.org/10.1016/j.atmosenv.2015.01.035.
(25) Kharol, S. K.; Martin, R. V.; Philip, S.; Boys, B.; Lamsal, L. N.; Jerrett, M.; Brauer, M.; Crouse, D. L.; McLinden, C.; Burnett, R. T. Assessment of the Magnitude and Recent Trends in Satellite-Derived Ground-Level Nitrogen Dioxide over North America. *Atmos. Environ.* **2015**, *118*, 236–245. https://doi.org/10.1016/j.atmosenv.2015.08.011.
(26) Henneman, L. R. F.; Shen, H.; Hogrefe, C.; Russell, A. G.; Zigler, C. M. Four Decades of United States Mobile Source Pollutants: Spatial–Temporal Trends Assessed by Ground-Based Monitors, Air Quality Models, and Satellites. *Environ. Sci. Technol.* **2021**, *55* (2), 882–892. https://doi.org/10.1021/acs.est.0c07128.
(27) Goldberg, D. L.; Lu, Z.; Oda, T.; Lamsal, L. N.; Liu, F.; Griffin, D.; McLinden, C. A.; Krotkov, N. A.; Duncan, B. N.; Streets, D. G. Exploiting OMI NO2 Satellite Observations to Infer Fossil-Fuel CO2 Emissions from U.S. Megacities. *Sci. Total Environ.* **2019**, *695*, 133805. https://doi.org/10.1016/j.scitotenv.2019.133805.
(28) Zhang, R.; Wang, Y.; Smeltzer, C.; Qu, H.; Koshak, W.; Boersma, K. F. Comparing OMI-Based and EPA AQS in Situ NO2 Trends: Towards Understanding Surface NOx Emission Changes. *Atmospheric Meas. Tech.* **2018**, *11* (7), 3955–3967. https://doi.org/10.5194/amt-11-3955-2018.
(29) Curier, R. L.; Kranenburg, R.; Segers, A. J. S.; Timmermans, R. M. A.; Schaap, M. Synergistic Use of OMI NO2 Tropospheric Columns and LOTOS–EUROS to Evaluate the NOx Emission Trends across Europe. *Remote Sens. Environ.* **2014**, *149*, 58–69. https://doi.org/10.1016/j.rse.2014.03.032.
(30) Zara, M.; Boersma, K. F.; Eskes, H.; Denier van der Gon, H.; Vilà-Guerau de Arellano, J.; Krol, M.; van der Swaluw, E.; Schuch, W.; Velders, G. J. M. Reductions in Nitrogen Oxides over the Netherlands between 2005 and 2018 Observed from Space and on the Ground: Decreasing Emissions and Increasing O3 Indicate Changing NOx Chemistry. *Atmospheric Environ. X* **2021**, *9*, 100104. https://doi.org/10.1016/j.aeaoa.2021.100104.
(31) Itahashi, S.; Yumimoto, K.; Kurokawa, J.; Morino, Y.; Nagashima, T.; Miyazaki, K.; Maki, T.; Ohara, T. Inverse Estimation of NOx Emissions over China and India 2005–2016: Contrasting Recent Trends and Future Perspectives. *Environ. Res. Lett.* **2019**, *14* (12), 124020. https://doi.org/10.1088/1748-9326/ab4d7f.
(32) Barkley, M. P.; González Abad, G.; Kurosu, T. P.; Spurr, R.; Torbatian, S.; Lerot, C. OMI Air-Quality Monitoring over the Middle East. *Atmospheric Chem. Phys.* **2017**, *17* (7), 4687–4709. https://doi.org/10.5194/acp-17-4687-2017.
(33) de Foy, B.; Lu, Z.; Streets, D. G. Satellite NO2 Retrievals Suggest China Has Exceeded Its NOx Reduction Goals from the Twelfth Five-Year Plan. *Sci. Rep.* **2016**, *6* (1), 35912. https://doi.org/10.1038/srep35912.
(34) Liu, F.; Beirle, S.; Zhang, Q.; van der A, R. J.; Zheng, B.; Tong, D.; He, K. NOx Emission Trends over Chinese Cities Estimated from OMI Observations during 2005 to 2015.

Atmospheric Chem. Phys. **2017**, *17* (15), 9261–9275. https://doi.org/10.5194/acp-17-9261-2017.

(35) Zheng, B.; Tong, D.; Li, M.; Liu, F.; Hong, C.; Geng, G.; Li, H.; Li, X.; Peng, L.; Qi, J.; Yan, L.; Zhang, Y.; Zhao, H.; Zheng, Y.; He, K.; Zhang, Q. Trends in China's Anthropogenic Emissions since 2010 as the Consequence of Clean Air Actions. *Atmospheric Chem. Phys.* **2018**, *18* (19), 14095–14111. https://doi.org/10.5194/acp-18-14095-2018.

(36) Leue, C.; Wenig, M.; Wagner, T.; Klimm, O.; Platt, U.; Jähne, B. Quantitative Analysis of NOs Emissions from Global Ozone Monitoring Experiment Satellite Image Sequences. *J. Geophys. Res. Atmospheres* **2001**, *106* (D6), 5493–5505. https://doi.org/10.1029/2000JD900572.

(37) van der A, R. J.; Eskes, H. J.; Boersma, K. F.; van Noije, T. P. C.; Van Roozendael, M.; De Smedt, I.; Peters, D. H. M. U.; Meijer, E. W. Trends, Seasonal Variability and Dominant NOx Source Derived from a Ten Year Record of NO2 Measured from Space. *J. Geophys. Res.* **2008**, *113* (D4), D04302. https://doi.org/10.1029/2007JD009021.

(38) Duncan, B. N.; Lamsal, L. N.; Thompson, A. M.; Yoshida, Y.; Lu, Z.; Streets, D. G.; Hurwitz, M. M.; Pickering, K. E. A Space-Based, High-Resolution View of Notable Changes in Urban NOx Pollution around the World (2005-2014). *J. Geophys. Res. Atmospheres* **2016**, *121* (2), 976–996. https://doi.org/10.1002/2015JD024121.

(39) Anenberg, S. C.; Bindl, M.; Brauer, M.; Castillo, J. J.; Cavalieri, S.; Duncan, B. N.; Fiore, A. M.; Fuller, R.; Goldberg, D. L.; Henze, D. K.; Hess, J.; Holloway, T.; James, P.; Jin, X.; Kheirbek, I.; Kinney, P. L.; Liu, Y.; Mohegh, A.; Patz, J.; Jimenez, M. P.; Roy, A.; Tong, D.; Walker, K.; Watts, N.; West, J. J. Using Satellites to Track Indicators of Global Air Pollution and Climate Change Impacts: Lessons Learned from a NASA-supported Science-stakeholder Collaborative. *GeoHealth* **2020**. https://doi.org/10.1029/2020GH000270.

(40) Griffin, D.; Zhao, X.; McLinden, C. A.; Boersma, F.; Bourassa, A.; Dammers, E.; Degenstein, D.; Eskes, H.; Fehr, L.; Fioletov, V.; Hayden, K.; Kharol, S. K.; Li, S.; Makar, P.; Martin, R. V.; Mihele, C.; Mittermeier, R. L.; Krotkov, N.; Sneep, M.; Lamsal, L. N.; Linden, M. ter; Geffen, J. van; Veefkind, P.; Wolde, M. High-Resolution Mapping of Nitrogen Dioxide With TROPOMI: First Results and Validation Over the Canadian Oil Sands. *Geophys. Res. Lett.* **2019**, *46* (2), 1049–1060. https://doi.org/10.1029/2018GL081095.

(41) Goldberg, D. L.; Anenberg, S. C.; Kerr, G. H.; Mohegh, A.; Lu, Z.; Streets, D. G. TROPOMI NO2 in the United States: A Detailed Look at the Annual Averages, Weekly Cycles, Effects of Temperature, and Correlation With Surface NO2 Concentrations. *Earths Future* **2021**, *9* (4). https://doi.org/10.1029/2020EF001665.

(42) Larkin, A.; Geddes, J. A.; Martin, R. V.; Xiao, Q.; Liu, Y.; Marshall, J. D.; Brauer, M.; Hystad, P. Global Land Use Regression Model for Nitrogen Dioxide Air Pollution. *Environ. Sci. Technol.* **2017**, *51* (12), 6957–6964. https://doi.org/10.1021/acs.est.7b01148.

(43) Pesaresi, M.; Florczyk, A.; Schiavina, M.; Melchiorri, M.; Maffenini, L. GHS Settlement Grid, Updated and Refined REGIO Model 2014 in Application to GHS-BUILT R2018A and GHS-POP R2019A, Multitemporal (1975-1990-2000-2015), R2019A, 2019. https://doi.org/10.2905/42E8BE89-54FF-464E-BE7B-BF9E64DA5218.

(44) Gelaro, R.; McCarty, W.; Suárez, M. J.; Todling, R.; Molod, A.; Takacs, L.; Randles, C. A.; Darmenov, A.; Bosilovich, M. G.; Reichle, R.; Wargan, K.; Coy, L.; Cullather, R.; Draper, C.; Akella, S.; Buchard, V.; Conaty, A.; da Silva, A. M.; Gu, W.; Kim, G.-K.; Koster, R.;

Lucchesi, R.; Merkova, D.; Nielsen, J. E.; Partyka, G.; Pawson, S.; Putman, W.; Rienecker, M.; Schubert, S. D.; Sienkiewicz, M.; Zhao, B. The Modern-Era Retrospective Analysis for Research and Applications, Version 2 (MERRA-2). *J. Clim.* **2017**, *30* (14), 5419–5454. https://doi.org/10.1175/JCLI-D-16-0758.1.

(45) Tatem, A. J. WorldPop, Open Data for Spatial Demography. *Sci. Data* **2017**, *4* (1), 170004. https://doi.org/10.1038/sdata.2017.4.

(46) Cohen, A. J.; Brauer, M.; Burnett, R.; Anderson, H. R.; Frostad, J.; Estep, K.; Balakrishnan, K.; Brunekreef, B.; Dandona, L.; Dandona, R.; Feigin, V.; Freedman, G.; Hubbell, B.; Jobling, A.; Kan, H.; Knibbs, L.; Liu, Y.; Martin, R.; Morawska, L.; Pope, C. A.; Shin, H.; Straif, K.; Shaddick, G.; Thomas, M.; van Dingenen, R.; van Donkelaar, A.; Vos, T.; Murray, C. J. L.; Forouzanfar, M. H. Estimates and 25-Year Trends of the Global Burden of Disease Attributable to Ambient Air Pollution: An Analysis of Data from the Global Burden of Diseases Study 2015. *The Lancet* **2017**. https://doi.org/10.1016/S0140-6736(17)30505-6.

(47) Khreis, H.; Alotaibi, R.; Horney, J.; McConnell, R. The Impact of Baseline Incidence Rates on Burden of Disease Assessment of Air Pollution and Onset Childhood Asthma: Analysis of Data from the Contiguous United States. *Ann. Epidemiol.* **2021**, *53*, 76-88.e10. https://doi.org/10.1016/j.annepidem.2020.08.063.

(48) Bechle, M. J.; Millet, D. B.; Marshall, J. D. National Spatiotemporal Exposure Surface for NO_2: Monthly Scaling of a Satellite-Derived Land-Use Regression, 2000–2010. *Environ. Sci. Technol.* **2015**, *49* (20), 12297–12305. https://doi.org/10.1021/acs.est.5b02882.

(49) Lee, H. J.; Koutrakis, P. Daily Ambient NO_2 Concentration Predictions Using Satellite Ozone Monitoring Instrument NO_2 Data and Land Use Regression. *Environ. Sci. Technol.* **2014**, 140204134232009. https://doi.org/10.1021/es404845f.

(50) Jamali, S.; Klingmyr, D.; Tagesson, T. Global-Scale Patterns and Trends in Tropospheric NO2 Concentrations, 2005–2018. *Remote Sens.* **2020**, *12* (21), 3526. https://doi.org/10.3390/rs12213526.

(51) Qu, Z.; Henze, D. K.; Cooper, O. R.; Neu, J. L. *Improving NO2 and Ozone Simulations through Global NOx Emission Inversions*; preprint; Gases/Atmospheric Modelling/Troposphere/Chemistry (chemical composition and reactions), 2020. https://doi.org/10.5194/acp-2020-307.

(52) Hickman, J. E.; Andela, N.; Tsigaridis, K.; Galy-Lacaux, C.; Ossohou, M.; Bauer, S. E. Reductions in NO2 Burden over North Equatorial Africa from Decline in Biomass Burning in Spite of Growing Fossil Fuel Use, 2005 to 2017. *Proc. Natl. Acad. Sci.* **2021**, *118* (7), e2002579118. https://doi.org/10.1073/pnas.2002579118.

(53) Barrington-Leigh, C.; Millard-Ball, A. Global Trends toward Urban Street-Network Sprawl. *Proc. Natl. Acad. Sci.* **2020**, *117* (4), 1941–1950. https://doi.org/10.1073/pnas.1905232116.

(54) GBD 2019 Diseases and Injuries Collaborators. Global Burden of 369 Diseases and Injuries in 204 Countries and Territories, 1990–2019: A Systematic Analysis for the Global Burden of Disease Study 2019. *The Lancet* **2020**, *396* (10258), 1204–1222. https://doi.org/Global burden of 369 diseases and injuries in 204 countries and territories, 1990–2019: a systematic analysis for the Global Burden of Disease Study 2019.

(55) Rodriguez, A.; Brickley, E.; Rodrigues, L.; Normansell, R. A.; Barreto, M.; Cooper, P. J. Urbanisation and Asthma in Low-Income and Middle-Income Countries: A Systematic

Review of the Urban–Rural Differences in Asthma Prevalence. *Thorax* **2019**, *74* (11), 1020–1030. https://doi.org/10.1136/thoraxjnl-2018-211793.

(56) Keet, C. A.; Matsui, E. C.; McCormack, M. C.; Peng, R. D. Urban Residence, Neighborhood Poverty, Race/Ethnicity, and Asthma Morbidity among Children on Medicaid. *J. Allergy Clin. Immunol.* **2017**, *140* (3), 822–827. https://doi.org/10.1016/j.jaci.2017.01.036.

Figures

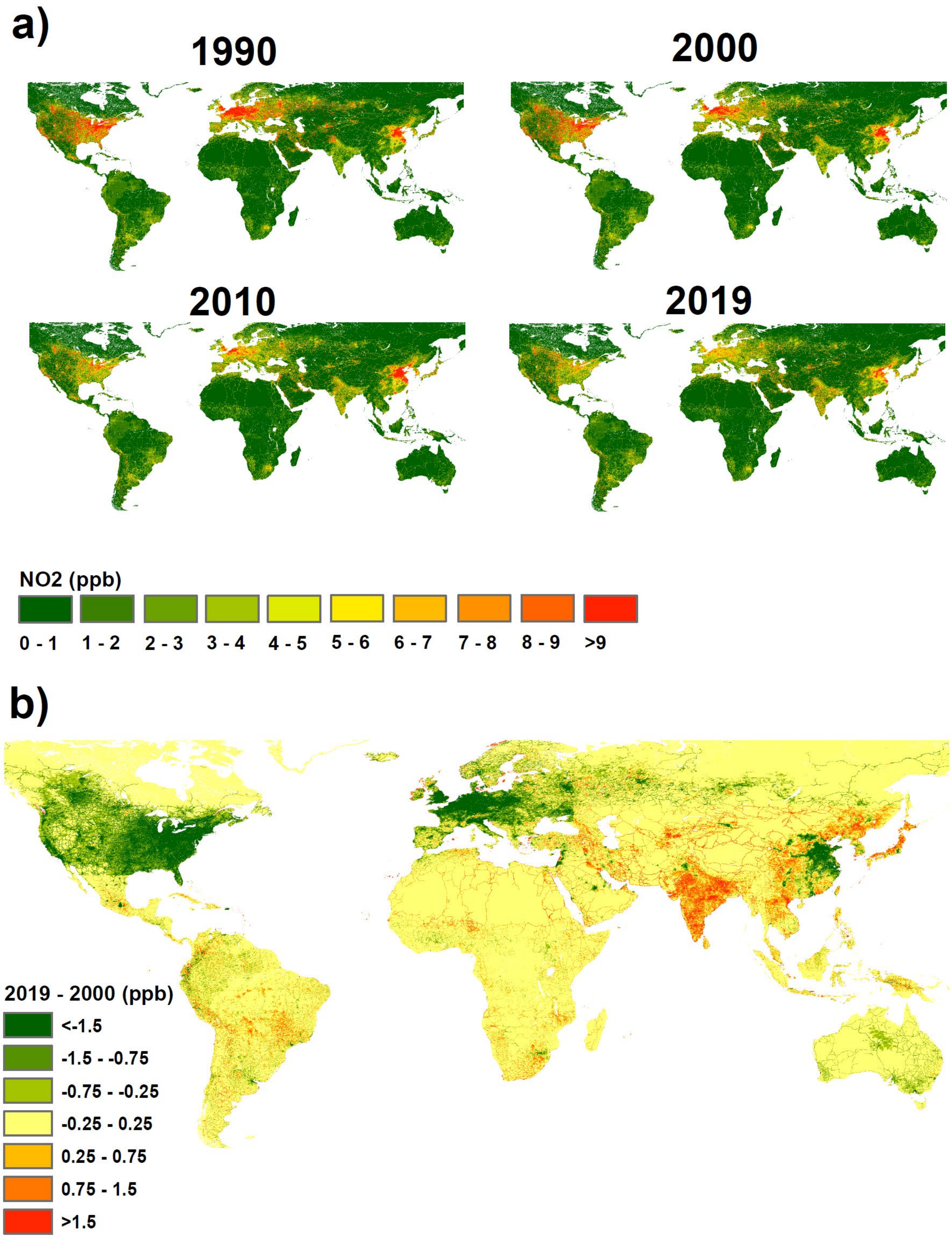

Figure 1. Annual average NO_2 concentrations at 1km x 1km resolution in a) 1990, 2000, 2010 and 2019 and b) difference between 2019 and 2000.

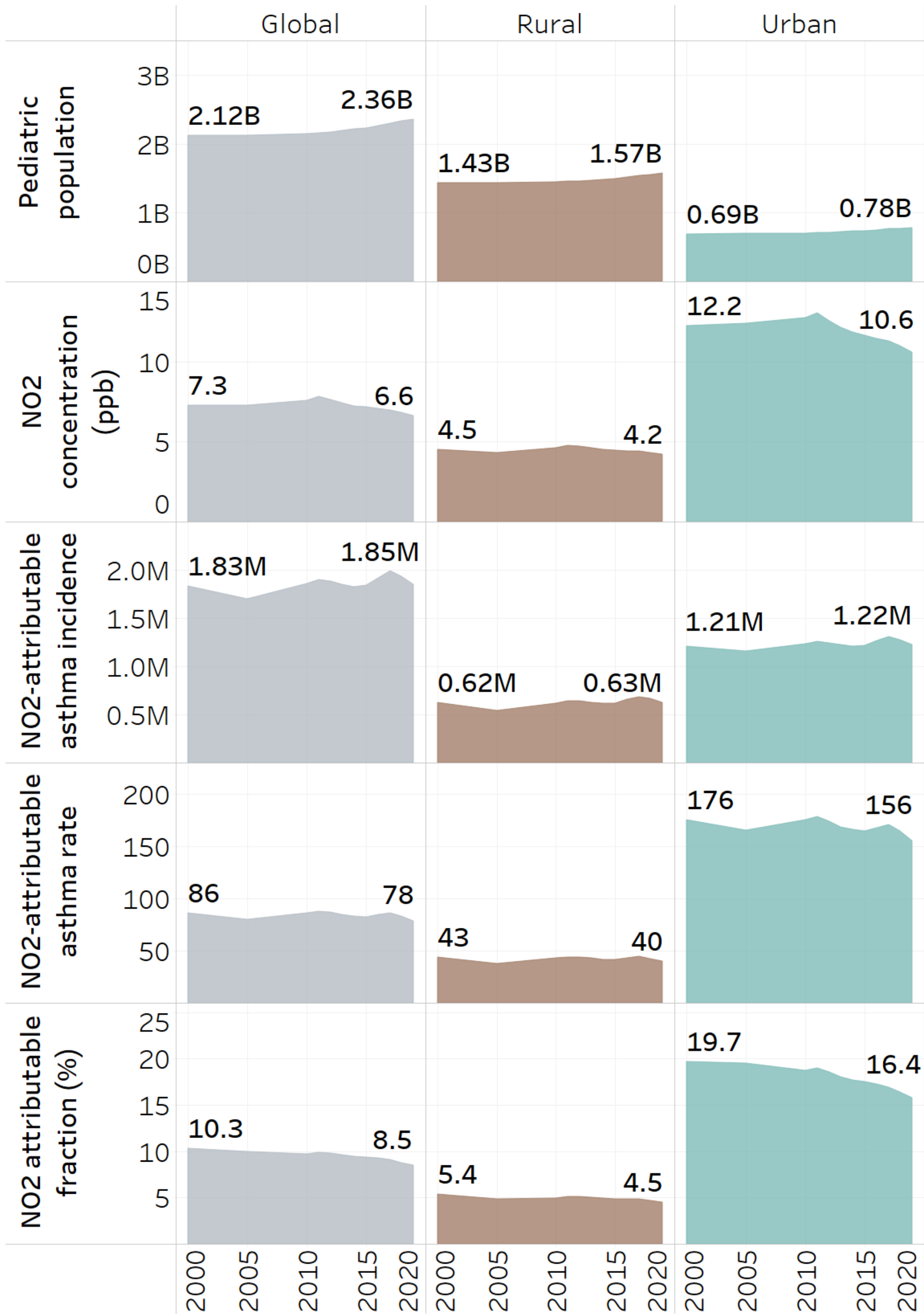

Figure 2. Trends (2000-2019) in population-weighted annual average NO_2 concentrations (ppb), NO_2-attributable pediatric asthma incidence, NO_2-attributable pediatric asthma incidence rate (per 100,000 children), and NO_2 attributable fraction globally (%), in all rural areas, and in 13,189 urban areas. Uncertainty intervals for NO_2-attributable pediatric asthma incidence are not shown since they are based on error in the relative risk estimate, which is constant over time.

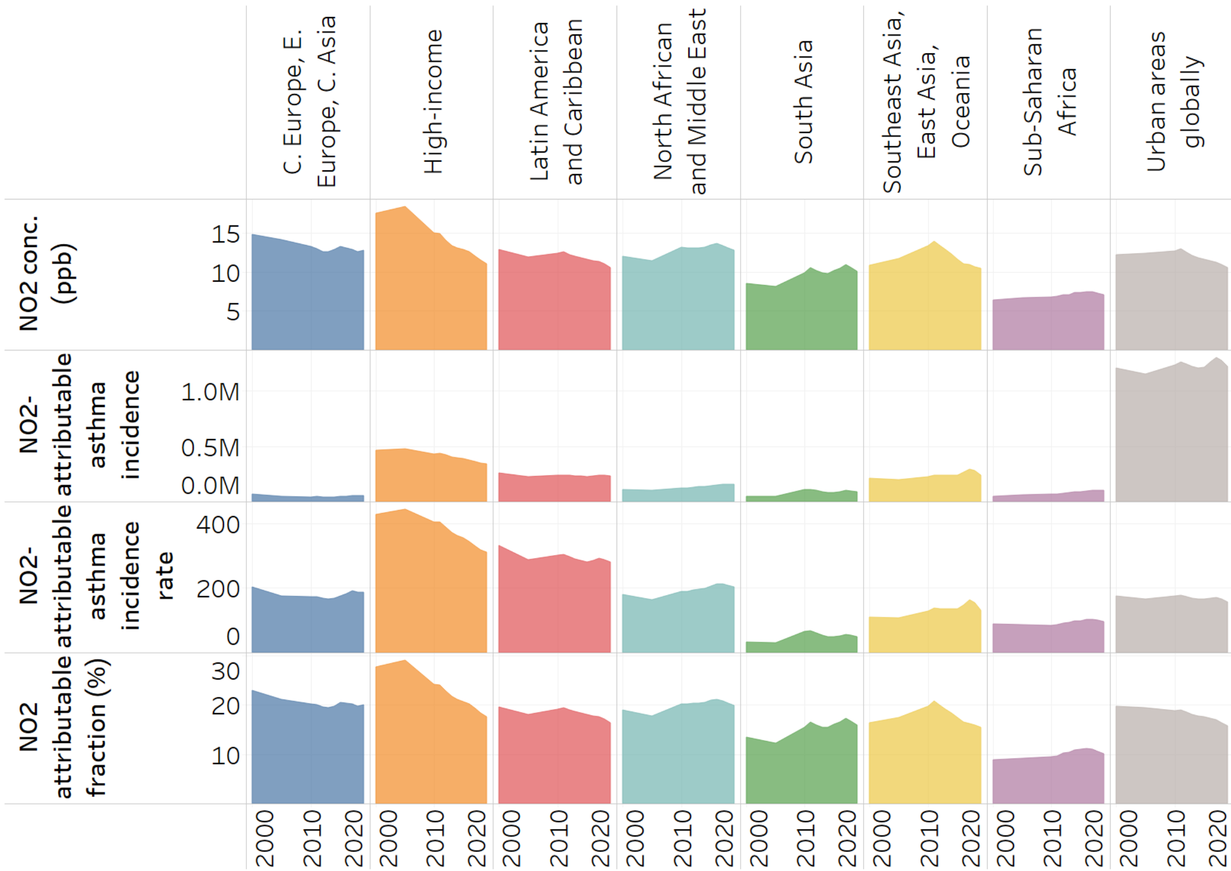

Figure 3. Trends (2000-2019) in population-weighted annual average NO_2 concentrations (ppb), NO_2-attributable pediatric asthma incidence (cases), NO_2-attributable pediatric asthma rates (per 100,000 children), and NO_2 attributable fraction (% of all pediatric asthma incidence) in urban areas in each sub-region. Results for each subregion within each super-region are shown in Figure S8. Uncertainty intervals for NO_2-attributable pediatric asthma incidence are not shown since they are based on error in the relative risk estimate, which is constant over time.

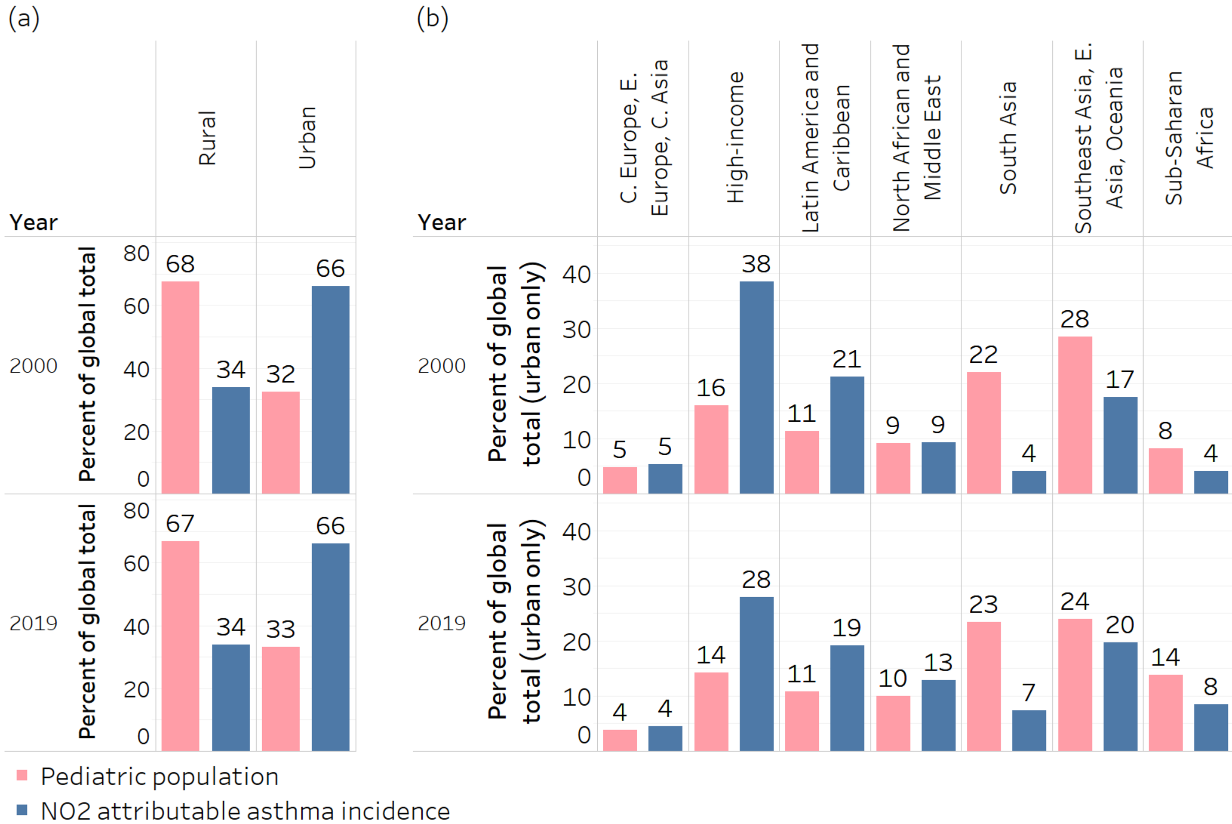

Figure 4. Percent of global total pediatric population and NO_2-attributable asthma cases in 2000 and 2019, for a) all rural areas and 13,189 urban areas globally, and b) urban areas within each region.

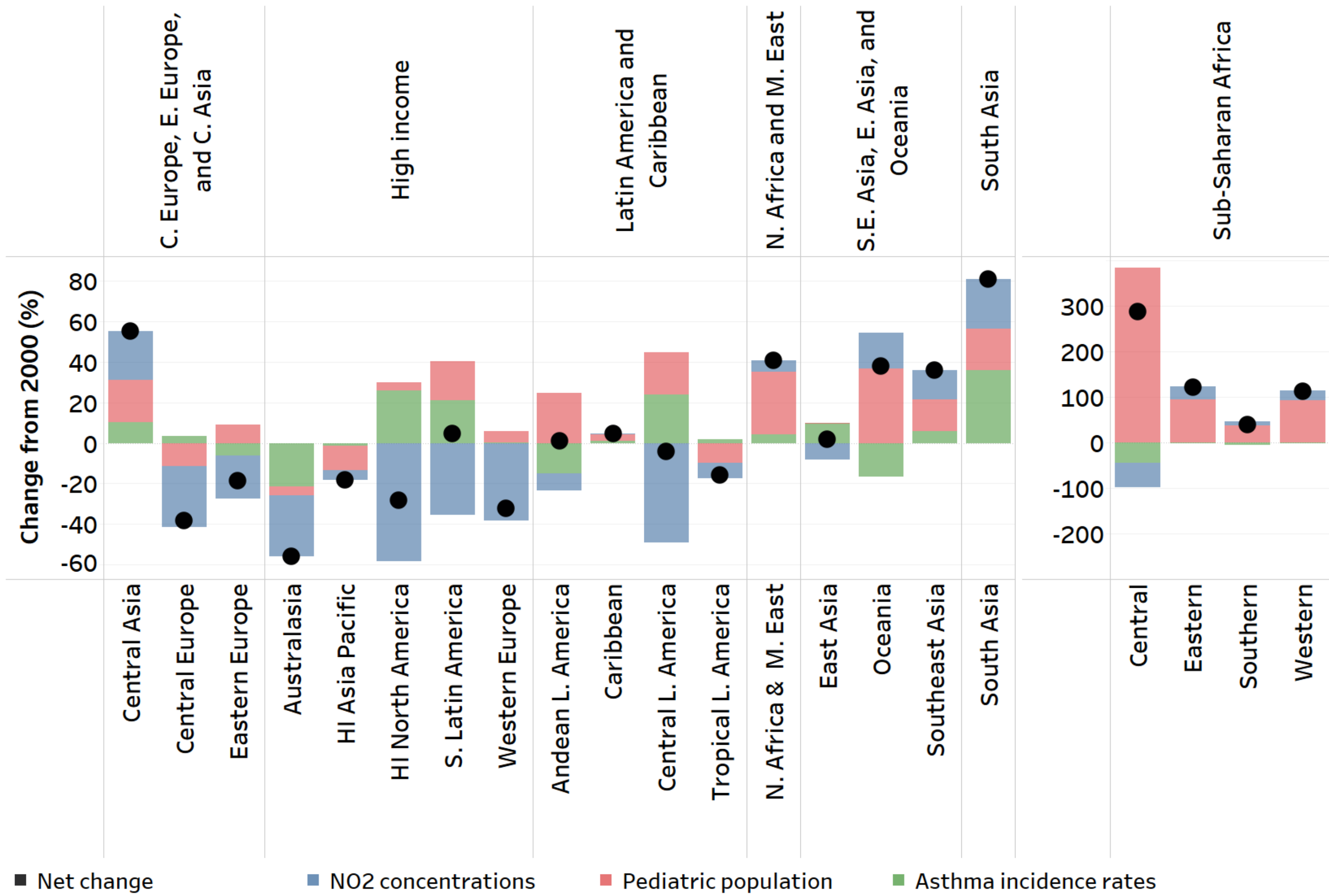

Figure 5. Contribution of pediatric population, baseline pediatric asthma rates, and NO_2 concentrations to changes in estimated NO_2-attributable pediatric asthma incidence between 2000 and 2019 for each sub-region. A different y-axis is used for regions in Sub-Saharan Africa. Results for the full time period are shown in Figure S11.

Supplemental material:

Long-term trends in urban NO_2 concentrations and associated pediatric asthma incidence: estimates from global datasets

Susan C. Anenberg, Arash Mohegh, Daniel L. Goldberg, Gaige H. Kerr, Michael Brauer, Katrin Burkart, Perry Hystad, Andrew Larkin, Sarah Wozniak, Lok Lamsal

Methods for adjusting surface NO_2 concentrations in rural areas

For grid cells >5km away from roadways and in rural areas, we developed new NO_2 concentration estimates using NO_2 column observations from the OMI satellite instrument with some adjustments to fill spatial and temporal gaps in the OMI satellite record, and to estimate 24-hour averages from the early afternoon OMI overpass time (Figure S1). We use an OMI NO_2 version 3, level 4 surface concentration dataset (0.1° x 0.1° resolution) for 2011, which followed methods described by Lamsal et al.[1] and was obtained from the NASA Goddard Space Flight Center (GSFC). The newer version 4 OMI retrieval uses enhanced surface reflectivities in the calculation of the tropospheric column amounts, but surface concentrations prepared by NASA GSFC are not currently available from the version 4 product. Due to the lack of satellite dataset coverage over snow/ice covered areas, some gridcells (mostly in higher latitudes) have no OMI observations in some months. We used the MERRA-2 reanalysis product (0.625° x 0.5° resolution) to generate a correction factor to ensure availability of NO_2 concentrations in all locations and months, as follows:

Equation S1: $$Correction\ factor\#1 = \frac{MERRA2_{annual\ averge}}{MERRA2_{average\ for\ same\ months\ that\ OMI\ level\ 4\ is\ available}}$$

We also applied a second correction factor to convert surface NO_2 concentrations from the early afternoon OMI overpass time (13:00 local time) to 24-hour averages. Following Anenberg et al.[2], we used NO_2 surface concentrations from the GMI-Replay chemical transport model[3,4] (2° x 2.5° resolution) simulations to generate these correction factors, as follows:

Equation S2: $$Correction\ factor\#2 = \frac{GMI_{24\ hour\ averge}}{GMI_{13:00}}$$

The NO_2 surface concentration estimates used for gridcells >5km away from roads and in rural areas were then generated using the following formula:

Equation S3: $$Adjusted\ rural\ concentrations = OMI\ level\ 4\ \times Correction\ factor\#1 \times Correction\ factor\ \#2$$

For rural gridcells within 5km of major roadways, we linearly scaled between Larkin et al.[5] values and the new adjusted rural concentrations in the span of the 5 km distance. The result of these steps is a 1km x 1km annual average surface NO_2 concentration dataset for 2011 that uses Larkin et al.[5] values in gridcells that are categorized as urban or over roads, and a new concentration dataset derived from OMI satellite observations in rural areas (Figure S2).

Methods for scaling NO_2 concentrations from 2011 to 1990-2019

The GBD requires NO_2 concentrations for each year included in the comparative risk assessment, from 1990-2019. We therefore scaled the new 2011 surface NO_2 concentration dataset to each year in this time period, in five-year increments from 1990-2005, and annually from 2010-2019. For the years 2005-2019, we scaled surface NO_2 concentrations from 2011 to each year using 3-year rolling averages of annual average NO_2 columns from the OMI version 4.0 level 2 product (13 km x 25 km resolution at nadir; Figure S3) at the gridcell level. We use NO_2 columns because surface concentrations derived from the version 4 OMI retrieval are not yet available. We oversampled the column NO_2 dataset to 0.1° x 0.1° resolution and re-gridded to 0.0083° x 0.0083° (approximately 1km x 1km). The 3-year rolling averages remove noise from the satellite data. For 2005 and 2019, we did not have data to create 3-year rolling averages, so we used that year's NO_2 columns directly. The years 1990, 1995, and 2000 predated the OMI observational record. We therefore used NO_2 concentrations from the MERRA-2 reanalysis product to scale 2011 NO_2 concentrations to those years.[6] To remove model noise, we created the MERRA-2 scaling factors across broad world regions (Figure S5), as opposed to applying scaling factors on a gridcell by gridcell basis as we did for the OMI scaling.

The final result used for estimating the global burden of disease from NO_2 is a global, 0.0083° x 0.0083° (approximately 1km x 1km) resolution dataset of annual average surface NO_2 concentrations from 1990-2019 (Figure 1).

Evaluation of NO_2 concentration dataset

The Larkin et al.[5] NO_2 concentration dataset was evaluated extensively in that work and agreed well with ground observations in urban areas. Here we add two limited new analyses to evaluate the changes we made in rural areas and the scaling other years (focusing specifically on the latest year, 2019).

We evaluated the rural NO_2 concentration estimates using the European Monitoring and Evaluation Program (EMEP) ground monitoring dataset, which has a large number of stations in rural areas (Table S1 and Figure S6). Other ground monitoring datasets (e.g. from EPA) may have rural sites, but we found that most were located directly downwind from urban areas. For example, the average surface annual mean NO_2 concentration in rural areas in 2011 from the EPA network is 4.3 ppb, likely too high to represent true background concentrations. We aggregated the available monitoring stations for the year 2011 to calculate annual averages and used a set of criteria to filter for stations that mostly closely represent background concentrations: 1) Stations with >300 days of data (the threshold was selected based on the distribution in days available for stations); 2) Stations that are at least 500m away from roads; 3) Stations that are not in urban and suburban areas. After applying these criteria, 67 stations across Europe remained. The evaluation is performed based on the aggregated annual average surface NO_2 concentrations for each monitor, and the value of the gridcell corresponding to that monitor for both original exposure dataset and final product.

The evaluation results show that the newly developed NO_2 surface concentrations outperformed the Larkin et al.[5] concentrations in rural areas, based on Root Mean Squared Error (RMSE), Mean Absolute Error (MAE), Mean Bias (MB), and correlation with ground observations (Table S1). The slope of the best fitted line is improved from 1.41 to 1.10, and the mean ratio of estimated to observed concentrations is improved from 1.81 to 1.32 (Table S1 and Figure S6). The RMSE is reduced from 3.37 ppb to 2.26 ppb, and MAE is improved from 2.74 ppb to 1.72 ppb, and the MB is reduced from 2.40 ppb to 1.02 ppb. The correlation between the estimated surface concentrations and ground measurements is improved from Pearson correlation coefficient (R) of 0.51 in the original product to 0.58.

In addition to the comparison of our dataset with previously published NO_2 concentrations during their overlapping time period, we further test the fidelity of our dataset for a more recent year (Figure S7). We obtain annual average observations for 2019 from three different networks: the National Air Pollution Surveillance (NAPS) program in Canada[7], the Air Quality System (AQS) in the United States[8], and the European Environment Agency (EEA) in Europe.[9] These networks provide data from 4,348 individual monitors (181 NAPS, 466 AQS, and 3,701 EEA), and we compare each monitor's NO_2 concentration to the concentration in the gridcell co-located with each monitor for

2019. All monitor data for 2019 have passed several quality control tests and quality assurance assessments by the entities that disseminate these data.

The mean bias (normalized mean bias) was -2.27 ppb (-20.40%) in Europe, 1.69 ppb in the U.S. (20.79%), and 3.34 ppb (49.56%) in Canada across the three networks in 2019 (Figure S7b,e,h). In urban areas specifically, the mean bias was -2.87 (-22.51%) in Europe, 1.26 ppb (12.21%) in the U.S., and 3.93 ppb (50.14%) in Canada for an average of 0.77 ppb across these three networks (Figure S7c,f,i). The mean bias at rural sites averaged over the three networks is 1.56 ppb, similar in magnitude to the rural bias reported for 2010-2012 (compare Figure S7c,f,i with Table S1).

The high mean bias evident in the NAPS and AQS datasets (Figure S7b-c, e-f) could, in part, reflect known issues with NO_2 monitors, which have been reported to overestimate NO_2 concentrations by up to ~50% due to interference from reactive nitrogen compounds, especially at locations distant from NO_x sources.[10] Additionally, this high bias could also stem from monitors sited near traffic or other sources of NO_x emissions that may not be resolved in our ~1 km^2 dataset.

The paucity of monitors throughout large swaths of Canada and the United States (Figure S7a, d) and throughout the rest of the world inhibits a more in-depth performance assessment of our dataset and highlights the urgent need for more strategic and equitable monitoring of ambient air pollution (e.g. [11]).

Methods for decomposing parameter contributions to NO_2-attributable asthma trends

We calculate the contribution of each parameter used in health impact assessment (population, baseline asthma rates, and concentrations) using four sets of simulations:

- Control scenario, where we calculated the asthma cases for each year.
- Three "parameter rollback" simulations in which we revert one of the parameters (population, baseline asthma rates, or concentrations) to the base year 2000.

By comparing each of the three parameter rollback scenarios to the control scenario, we calculate the contribution of each parameter to the change in asthma cases between 2000 and all other years. We use the following set of equations to calculate the contribution of each parameter.

We use Equation S4 to calculate pediatric asthma incidence attributable to NO_2 for the control scenario. This equation is the same as Equation 1 in the main text, but we denote the parameters differently here to make it easier to compare with the control scenario equations.

Equation S4: $$Control_t(x_t, y_t, z_t) = x_t \times y_t \times z_t$$

Where $Control_t$ is the NO_2-attributable pediatric asthma incidence for year *t*, x_t is the baseline pediatric asthma rate for year *t*, y_t is the pediatric population for year *t*, and z_t is the fraction of pediatric asthma incidence that is attributable to NO_2 for year *t*.

We then calculate NO_2-attributable pediatric asthma incidence for each simulation, replacing one parameter with its value in the year 2000 while holding the other two parameters at the same value used in the control scenario (Equations S5-S7).

Equation S5: $$Simulation_{x,t}(x_0, y_t, z_t) = x_0 \times y_t \times z_t$$

Equation S6: $$Simulation_{y,t}(x_t, y_0, z_t) = x_t \times y_0 \times z_t$$

Equation S7: $$Simulation_{z,t}(x_t, y_t, z_0) = x_t \times y_t \times z_0$$

Where $Simulation_{i,t}$ is the estimated NO_2-attributable pediatric asthma incidence for year t, where we have reverted one parameter back to the base year of 2000.

We then calculate the ratio of estimated NO_2-attributable pediatric asthma incidence in the control scenario versus in each of the parameter rollback scenarios, as shown in Equation S8.

Equation S8: $$Ratio_{i,t} = \frac{Control_t}{Simulation_{i,t}}$$

Since NO_2-attributable pediatric asthma incidence is calculated by multiplying three parameters, we assume that the ratio of NO_2-attributable asthma incidence between year *t* and base year 2000 would be equivalent to the multiplication of the three rollback scenario ratios calculated in Equations S5-S7 (Equation S9). In this step we assume that aggregating the three parameter rollbacks separately is equivalent to reverting all of them together.

Equation S9: $$\frac{Asthma_t}{Asthma_0} \approx Ratio_{x,t} \times Ratio_{y,t} \times Ratio_{z,t}$$

To calculate the contribution of each parameter individually, we need to transform the parameter ratios so that they add up to 1 when summed. We therefore calculate a logarithm in the base of the left side of Equation S9 ($Asthma_t/Asthma_0$); since the logarithm of every number in its own base equals 1, this step makes the left side equal to 1 (Equation S10).

Equation S10: $$1 = \log(Ratio_{x,t}) + \log(Ratio_{y,t}) + \log(Ratio_{z,t})$$

Finally, we multiply each of the three log-transformed parameter rollback ratios by the total percentage change in NO_2-attributable asthma incidence between years 2000 and *t* to calculate the percent contribution of each parameter to that total change (Equation S11).

Equation S11: $$Contribution_{i,t} = \frac{Asthma_t}{Asthma_0} \times log(Ratio_{i,t})$$

Using this methodology, we calculated percent contributions for each of the three health impact function parameters (concentration, population, asthma rates) that add up to the total percentage changes between the two years, while remaining loyal to the multiplicative nature of the original health impact assessment function.

Supplemental Tables and Figures

Table S1. Statistical parameters for NO_2 concentrations from the Larkin et al.[5] dataset and our new concentration estimates for rural areas compared with EMEP rural observations. Values reported here for Larkin et al.[5] differ from those reported in their paper because here we are only evaluating predicted concentrations in rural areas at the EMEP monitor locations.

	Root Mean Square Error (RMSE) (ppb)	**Mean Absolute Error (MAE) (ppb)**	**Mean Bias (MB) (ppb)**	**Pearson coefficient (R)**	**Mean ratio: Estimate/obs**	**Slope of best fitted line**
New product	2.26	1.72	1.02	0.58	1.32	1.10
Larkin et al.[5]	3.37	2.74	2.40	0.51	1.81	1.41

Table S2. Count of urban clusters in each GBD region/super region. The total does not match the total urban clusters in analysis (13,189) since some urban clusters are located at the border between two regions.

Super region name	Region name	Count
Central Europe, Eastern Europe, and Central Asia		**628**
	Central Asia	148
	Central Europe	161
	Eastern Europe	319
High-income		**1280**
	Australasia	35
	High-income Asia Pacific	148
	High-income North America	389
	Southern Latin America	115
	Western Europe	593
Latin America and Caribbean		**968**
	Andean Latin America	93
	Caribbean	75
	Central Latin America	438
	Tropical Latin America	362
North Africa and Middle East		**1231**
	North Africa and Middle East	1231
South Asia		**3899**
	South Asia	3899
Southeast Asia, East Asia, and Oceania		**2904**
	East Asia	1955
	Oceania	49
	Southeast Asia	900
Sub-Saharan Africa		**2313**
	Central Sub-Saharan Africa	250
	Eastern Sub-Saharan Africa	1024
	Southern Sub-Saharan Africa	124
	Western Sub-Saharan Africa	915
Grand Total		**13223**

Table S3. Population-weighted NO_2 concentrations (ppb), NO_2-attributable pediatric asthma incidence (95% uncertainty interval in parentheses), NO_2-attributable pediatric asthma incidence rate (per 100,000), and NO_2 attributable fraction (%) for each super-region in 2000, 2005, 2010, and 2019.

Super region	Year	Pop-wt NO_2 concentration (ppb)	NO_2-attributable pediatric asthma incidence	NO_2-attributable asthma rate (per 100,000)	NO_2 attributable fraction
Central Europe, Eastern Europe, Central Asia	2000	15.1	65,000 (33,400 – 107,500)	202	23
	2010	13.6	44,300 (26,400 – 85,300)	172	20
	2019	12.7	54,900 (26,400 – 87,000)	188	20
High-income	2000	17.3	464,800 (264,700 – 725,800)	428	29
	2010	15.1	433,300 (255,500 – 655,000)	404	24
	2019	11.1	340,900 (191,400 – 523,200)	310	17
Latin America and Caribbean	2000	12.8	256,100 (147,300 – 397,000)	332	19
	2010	12.4	236,900 (138,000 – 380,300)	302	19
	2019	10.6	233,800 (125,300 – 375,800)	281	16
North Africa and Middle East	2000	12.1	111,800 (63,300 – 176,300)	180	19
	2010	13.2	120,100 (65,000 – 189,200)	189	20
	2019	12.8	157,600 (67,000 – 202,200)	203	20
South Asia	2000	8.6	50,000 (28,600 – 78,100)	33	13
	2010	9.9	106,500 (55,900 – 161,900)	65	15
	2019	10.1	90,400 (40,700 – 130,700)	50	16
Southeast Asia, East Asia, and Oceania	2000	11.1	211,300 (113,900 – 343,100)	109	16
	2010	14	226,600 (129,500 – 377,600)	128	18
	2019	10.6	240,900 (122,100 – 378,000)	129	15
Sub-Saharan Africa	2000	6.4	49,100 (27,400 – 78,700)	89	9
	2010	6.9	65,700 (26,000 – 74,700)	84	9
	2019	7.1	102,900 (30,200 – 90,900)	97	10

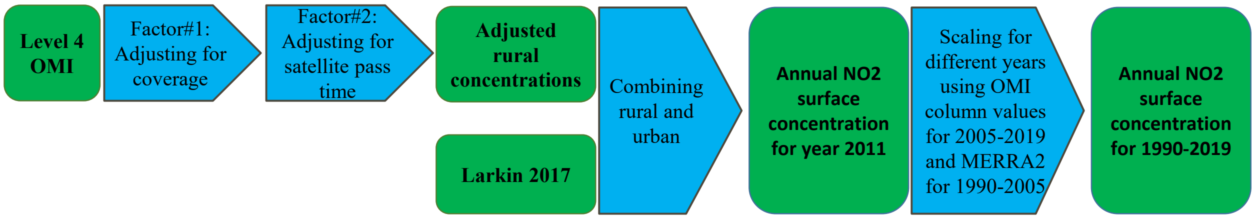

Figure S1. Schematic of datasets used and the process of combining them. Blue arrows represent applied processes.

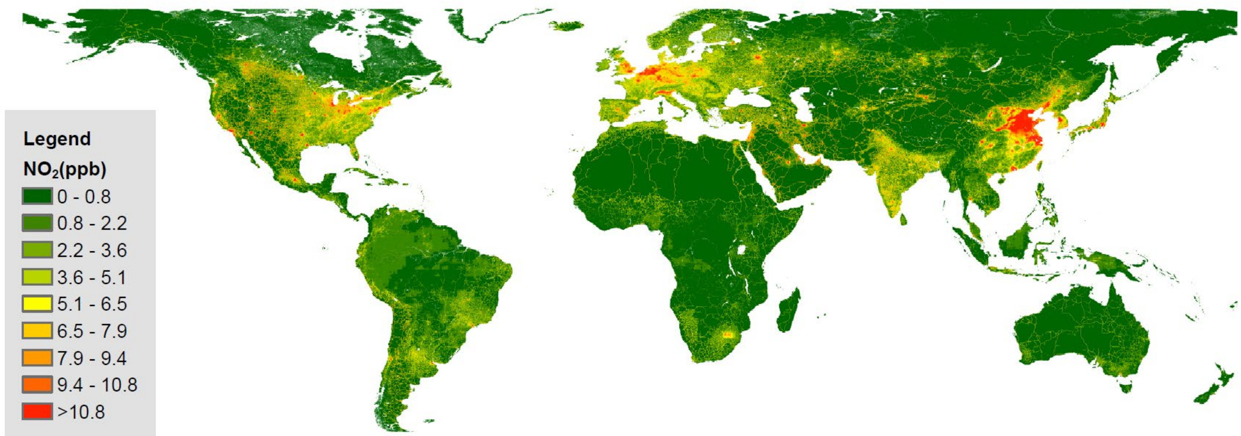

Figure S2. Annual average surface NO_2 concentration estimates for 2011 at ~1km x 1km resolution globally from this work, using a combination of Larkin et al.[5] land use regression estimates, OMI satellite observations, and chemical transport modeling.

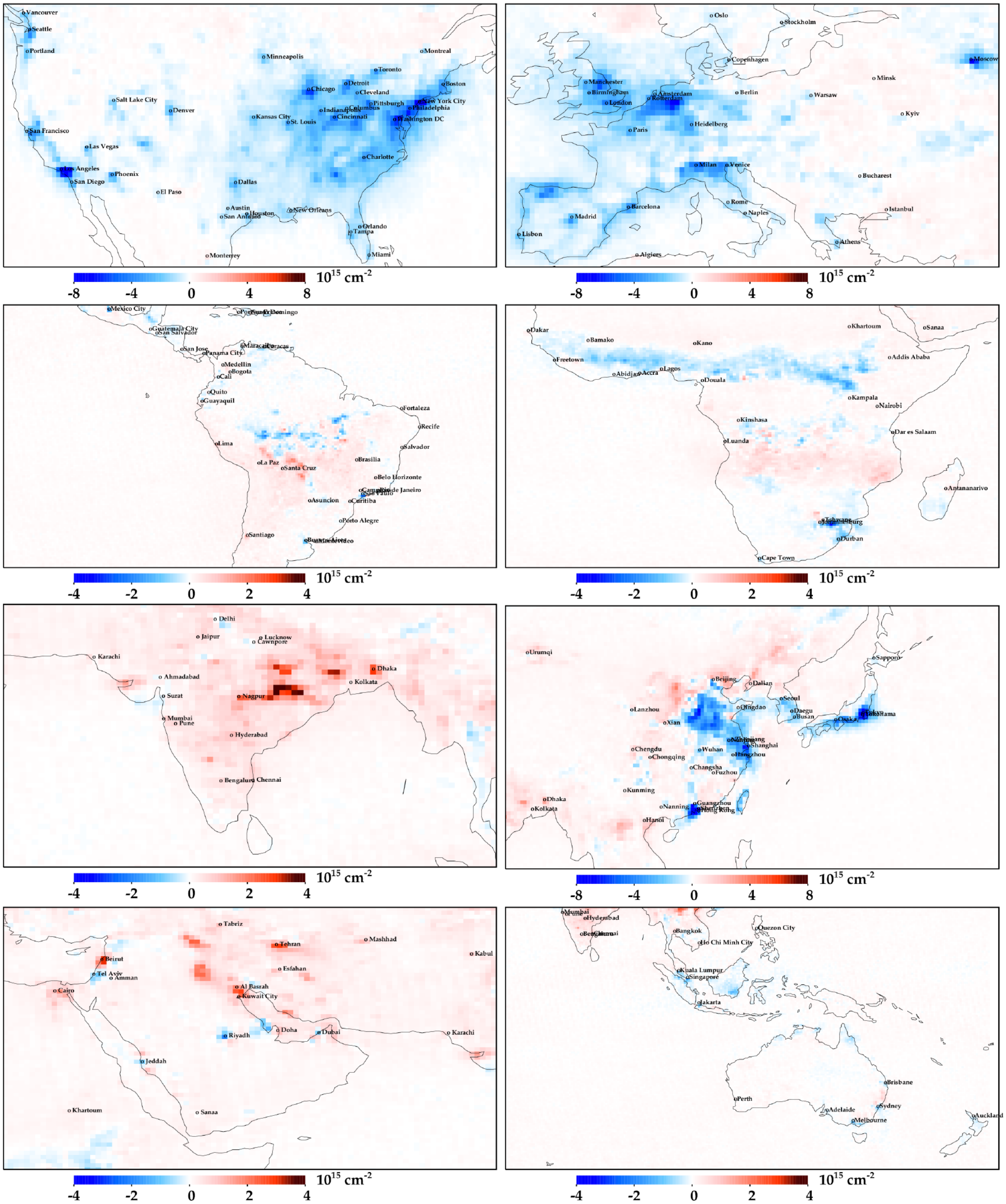

Figure S3. Regional trends in annual average NO_2 column densities (0.5° x 0.5°) from the OMI satellite instrument (2005-2019).

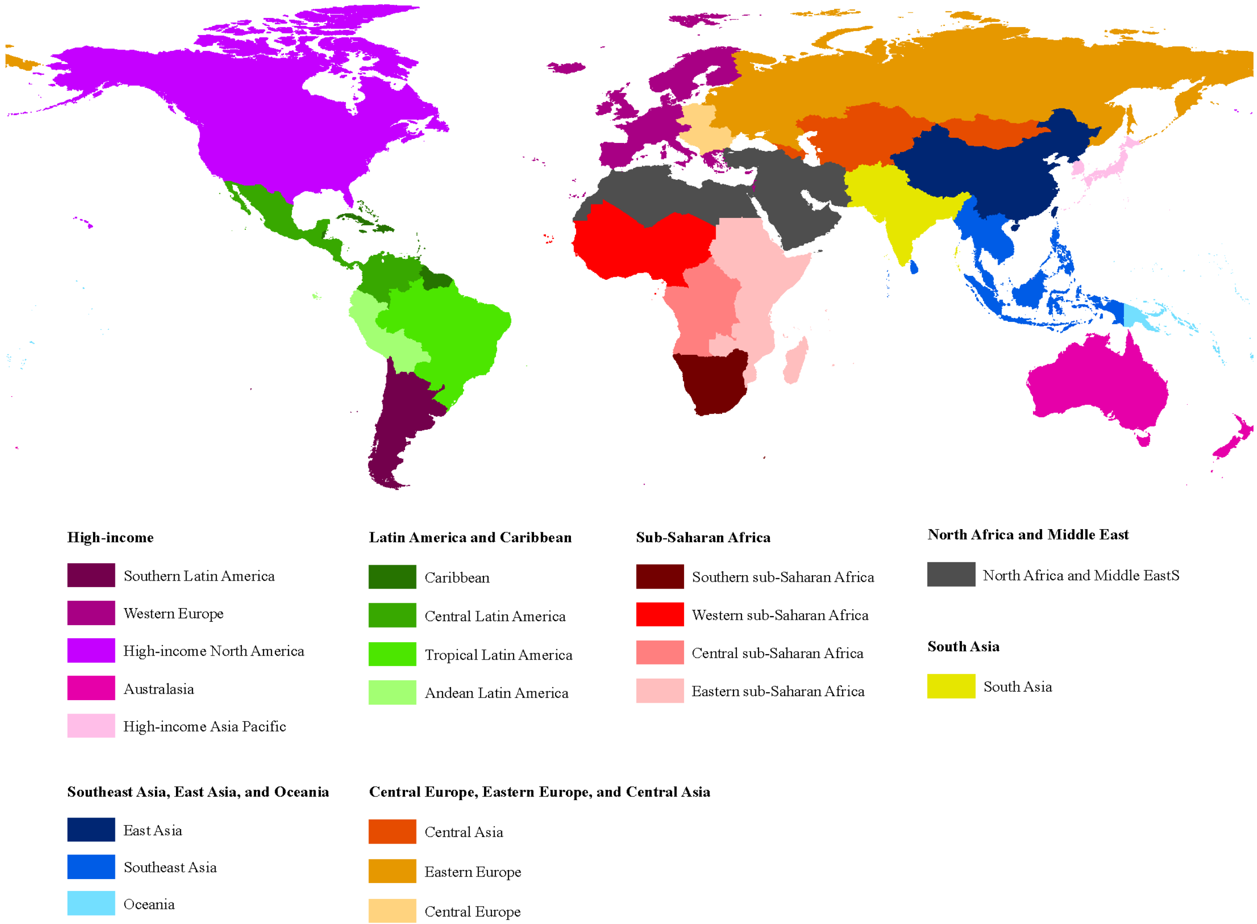

Figure S4. Countries and territories included in each region and super region, using regional definitions from the GBD 2019 Study.

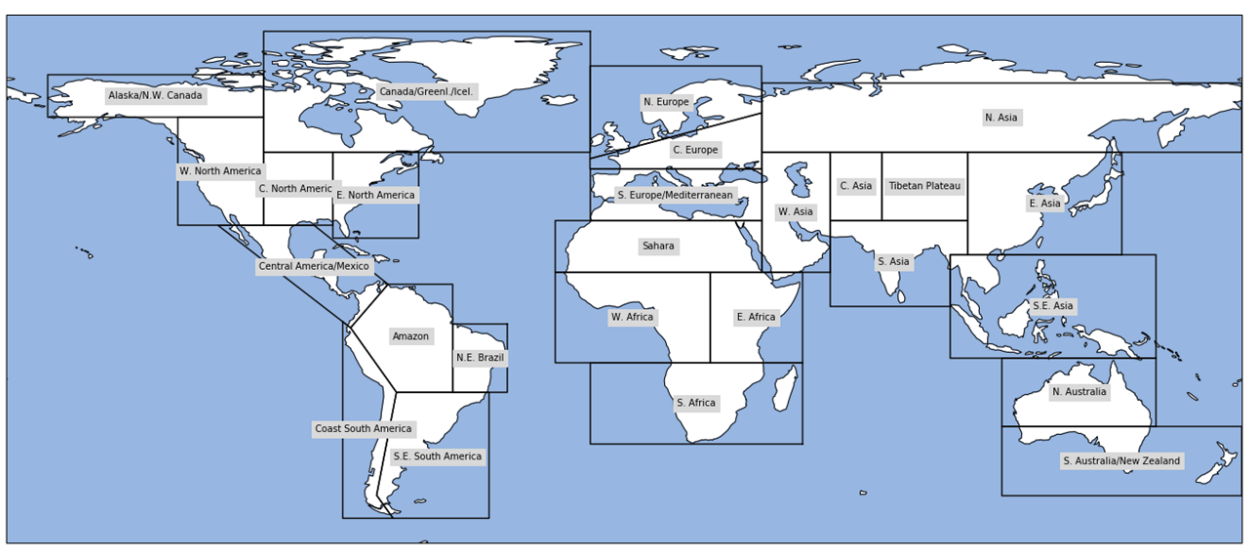

Figure S5. World regions used to generate the MERRA-2 scaling factors for NO_2 in 1990, 1995, and 2000.

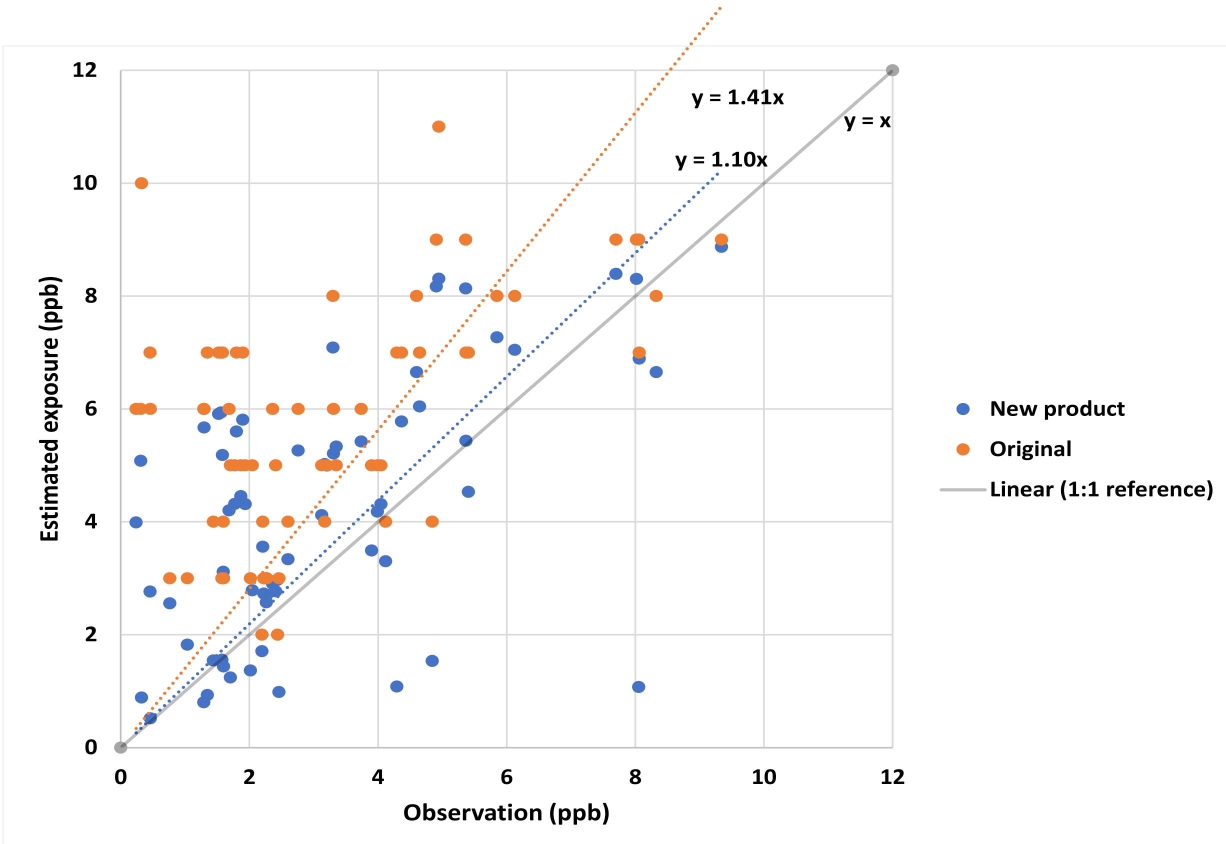

Figure S6. Comparison between annual average NO_2 concentrations from the original Larkin et al.[5] product (orange) and our new NO_2 concentration product (blue), versus concentrations from ground measurements for 2011 in rural areas. A 1:1 reference line is added for comparison. Each point represents a monitor. Monitor data source: European Monitoring and Evaluation Programme (EMEP).

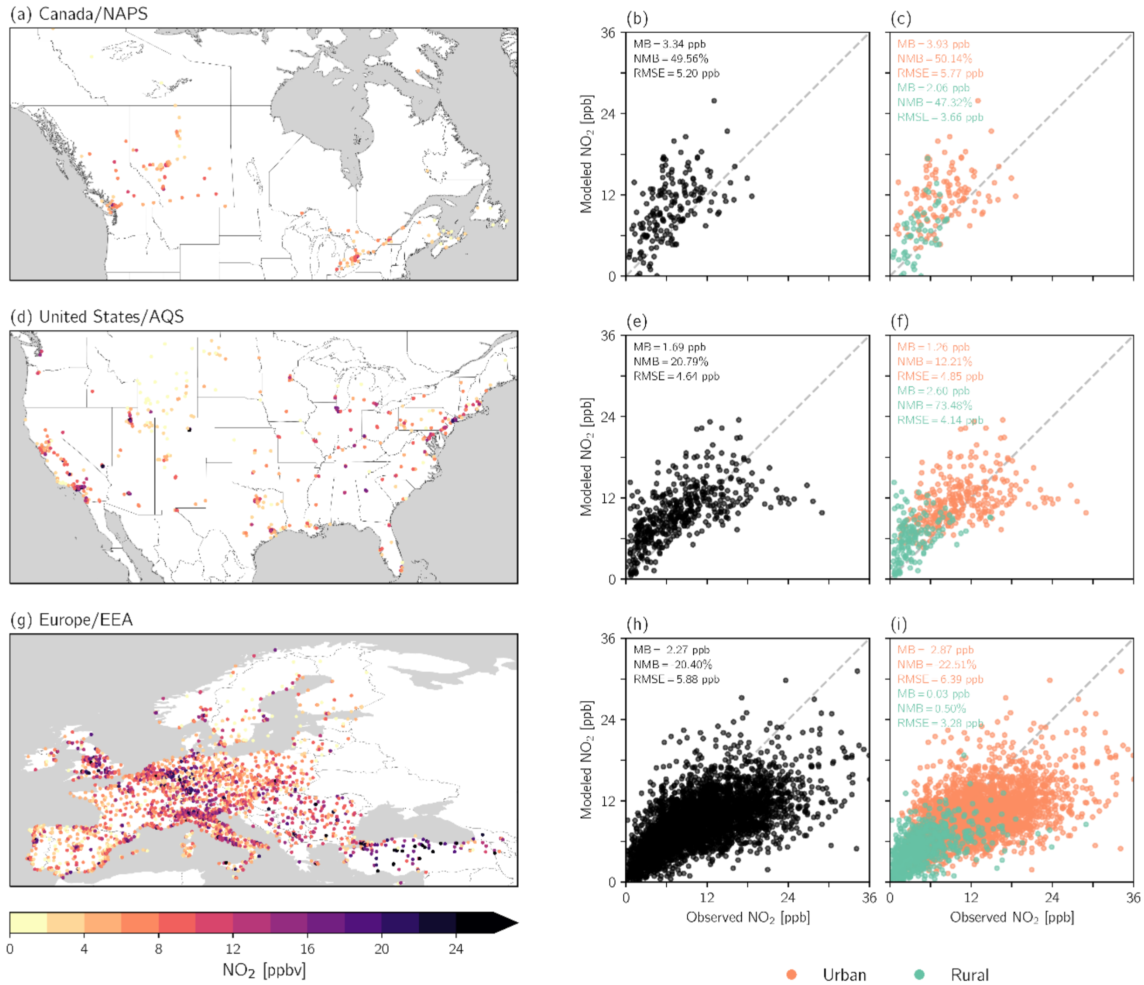

Figure S7. (a,d,g) The location of NO_2 monitors from the NAPS, AQS, and EEA networks and their annual average 2019 concentrations. (b,e,h) Annual average 2019 NO_2 concentrations from the gridcells co-located with each monitor versus the monitor concentrations. (c,f,i) are the same as (b,e,h) but for urban versus rural monitors. Rurality in (c,f,i) is determined with the GHS-SMOD dataset. The mean bias (MB; $= \bar{M} - \bar{O}$), normalized mean bias (NMB; $= (\frac{\bar{M}}{\bar{O}} - 1) \times 100\%$), and RMSE ($= \left[\frac{1}{N}\sum_{i=1}^{N} (M_i - O_i)^2\right]^{\frac{1}{2}}$) are indicated in each scatterplot. Here, M corresponds to the new dataset and O corresponds to observed concentrations. A 1:1 reference line is included in scatterplots for comparison.

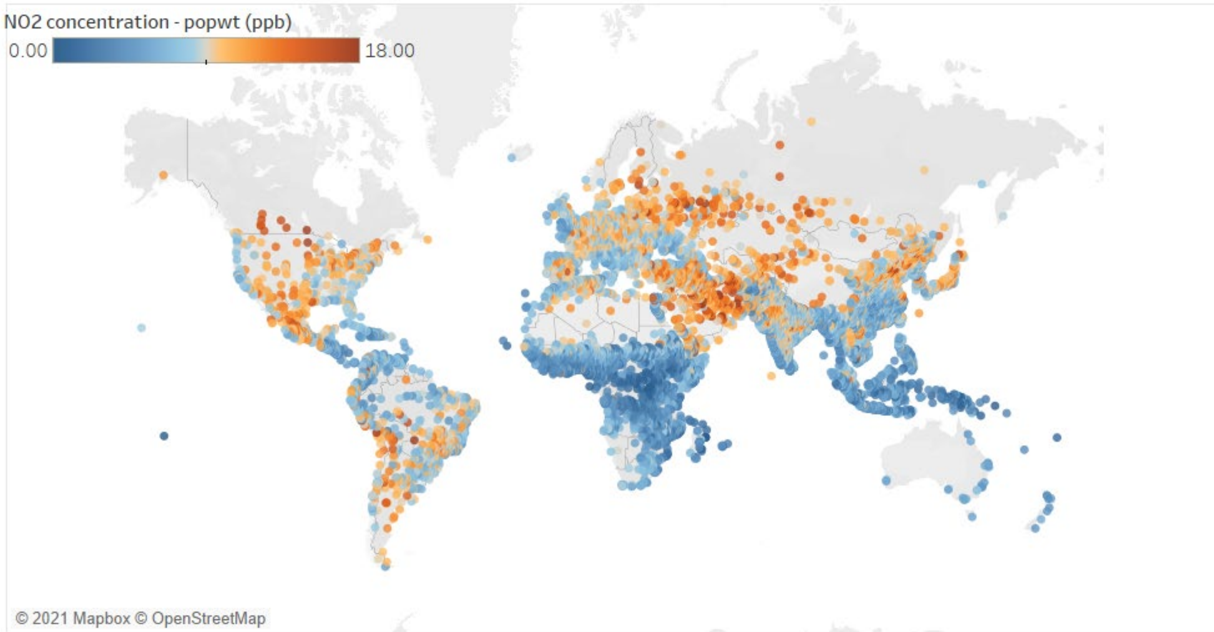

City Id	City Name	Sovereign	NO2 concentration (ppb)	NO2 concentration - popwt (ppb)
4355	Beirut	Lebanon	22.9	36.6
11392	Shenyang	China	18.6	22.5
12456	Shanghai	China	16.7	22.1
5703	Az Zubayr	Iraq	21.5	21.6
3686	Moscow	Russia	18.9	21.4
5767	Tehran	Iran	19.2	21.2
5451	Ad Diwaniyah	Iraq	20.1	21.0
4353	Saida	Lebanon	17.1	20.6
3407	Saint Petersburg	Russia	18.5	20.4
5908	Yazd	Iran	19.9	20.4

Figure S8. Population-weighted annual average NO_2 concentrations (ppb) for 13,189 urban areas (top) and the cities with the top 10 concentrations (bottom) in 2019. Color bar saturates at 18 ppb for greater contrast.

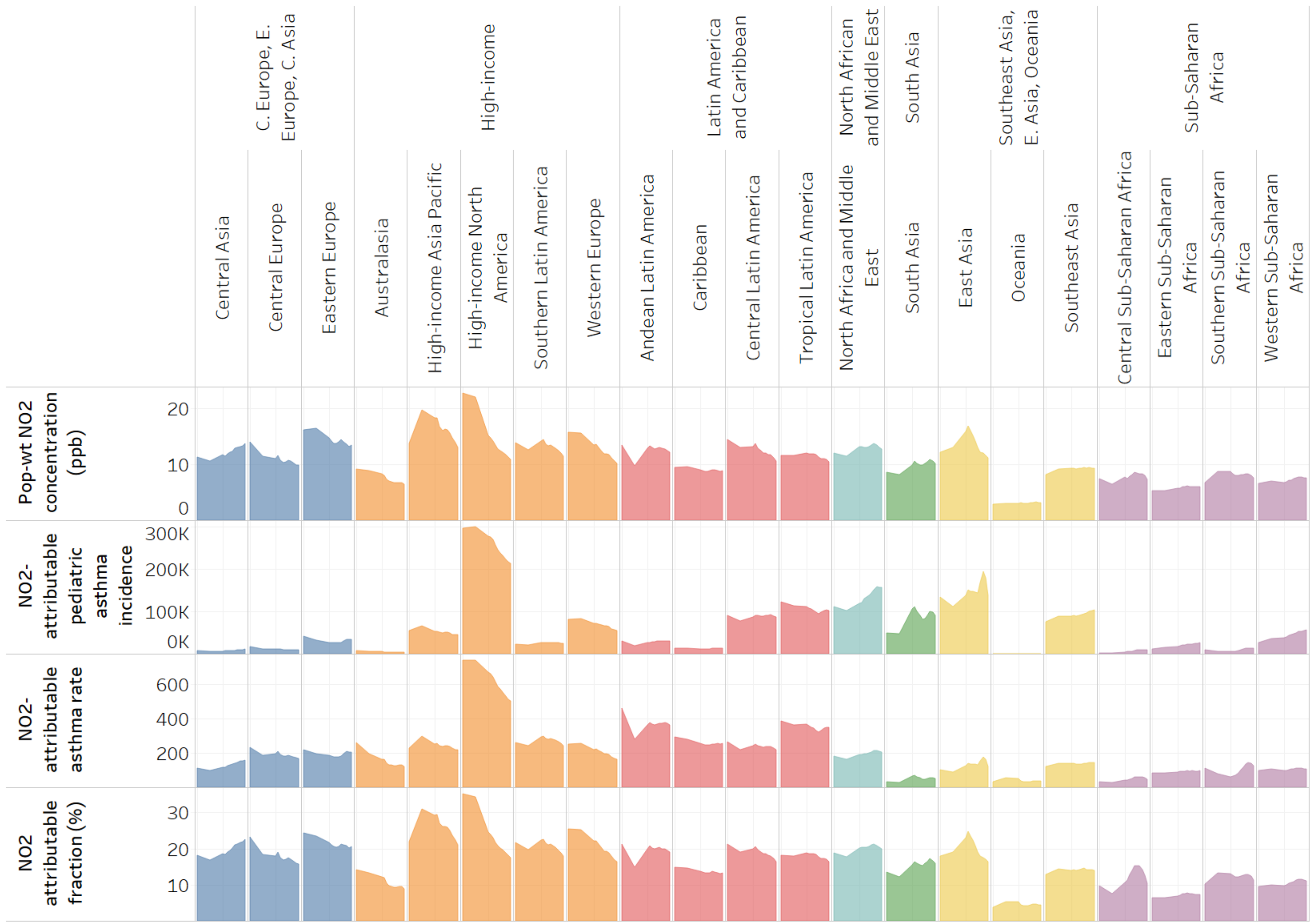

Figure S9. As for Figure 3, but for each subregion within each super-region.

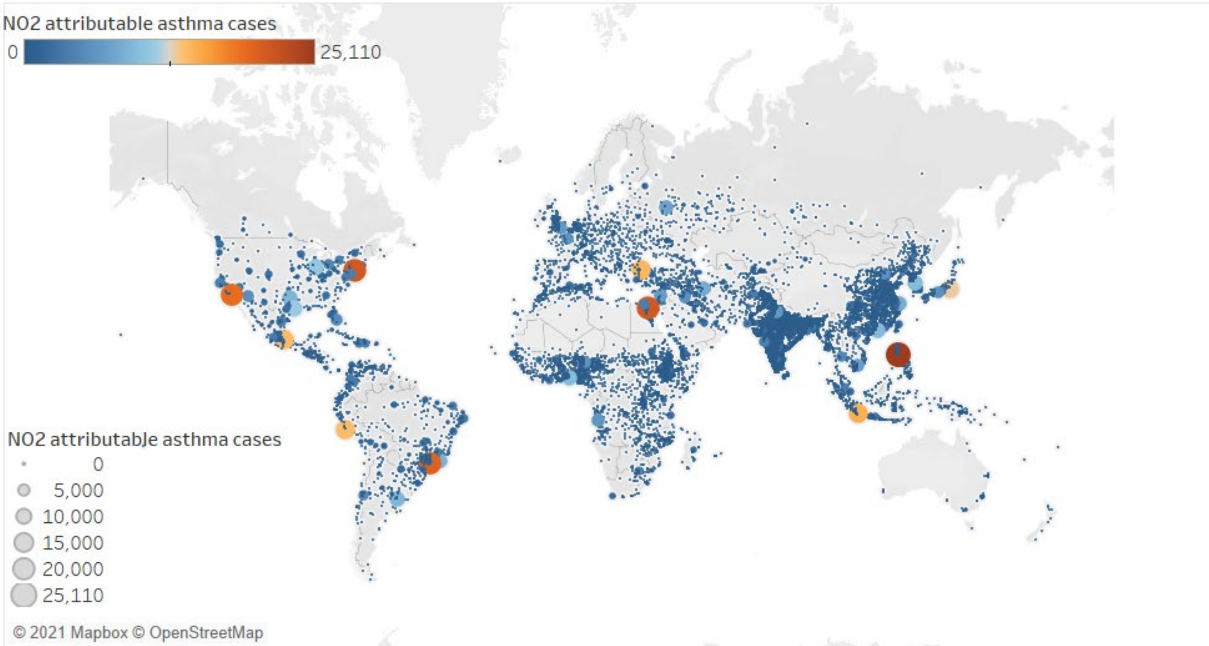

City Id	City Name	Sovereign	NO2 attributable asthma cases
12882	Quezon City [Manila]	Philippines	25,100
950	New York	United States of America	21,100
3915	Cairo	Egypt	21,100
1308	SÃo Paulo	Brazil	20,000
14	Los Angeles	United States of America	19,100
11920	Jakarta	Indonesia	14,800
3574	Istanbul	Turkey	14,400
155	Mexico City	Mexico	14,100
530	Lima	Peru	14,000
13017	Tokyo	Japan	13,100

Figure S10. As for Figure S8, but for NO_2-attributable pediatric asthma incidence.

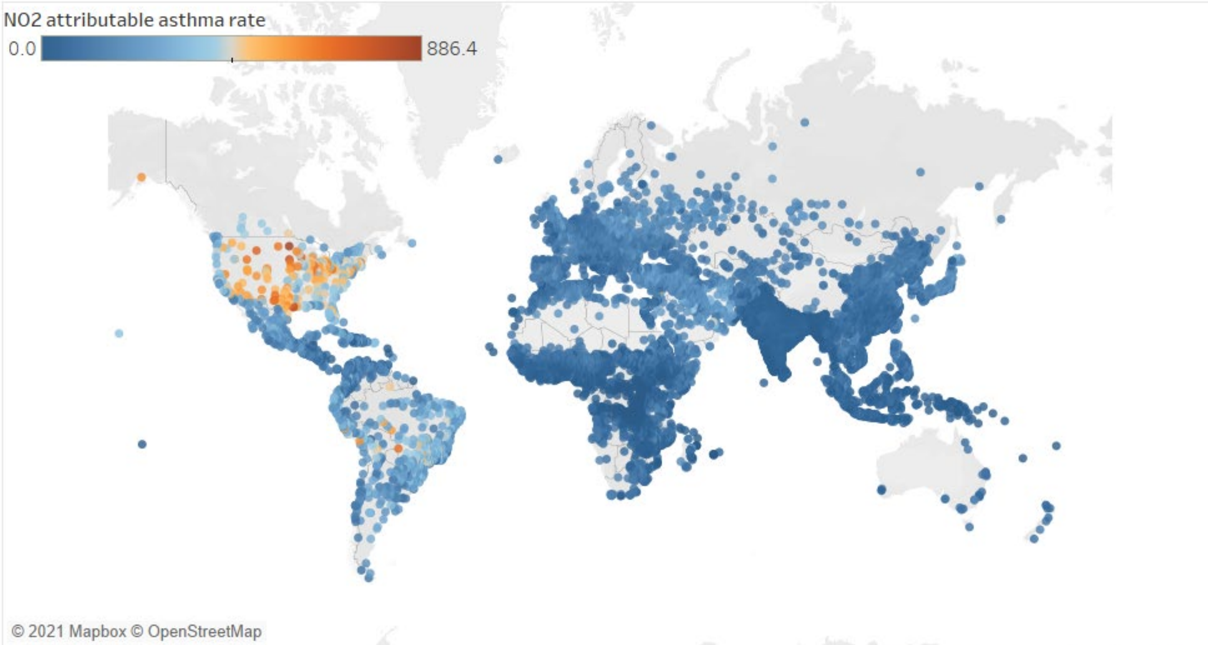

City Id	City Name	Sovereign	NO2-attributable pediatric asthma rate
512	Fargo	United States of America	886.4
451	Sioux Falls	United States of America	792.0
316	Houston	United States of America	773.3
333	Atascocita	United States of America	734.0
235	Midland	United States of America	724.8
568	Rochester	United States of America	717.1
339	Billings	United States of America	705.7
579	Bloomington	United States of America	679.0
639	Chicago	United States of America	679.0
1030	Lowell	United States of America	673.8

Figure S11. As for Figure S8, but for NO_2-attributable pediatric asthma incidence rate per 100,000 children.

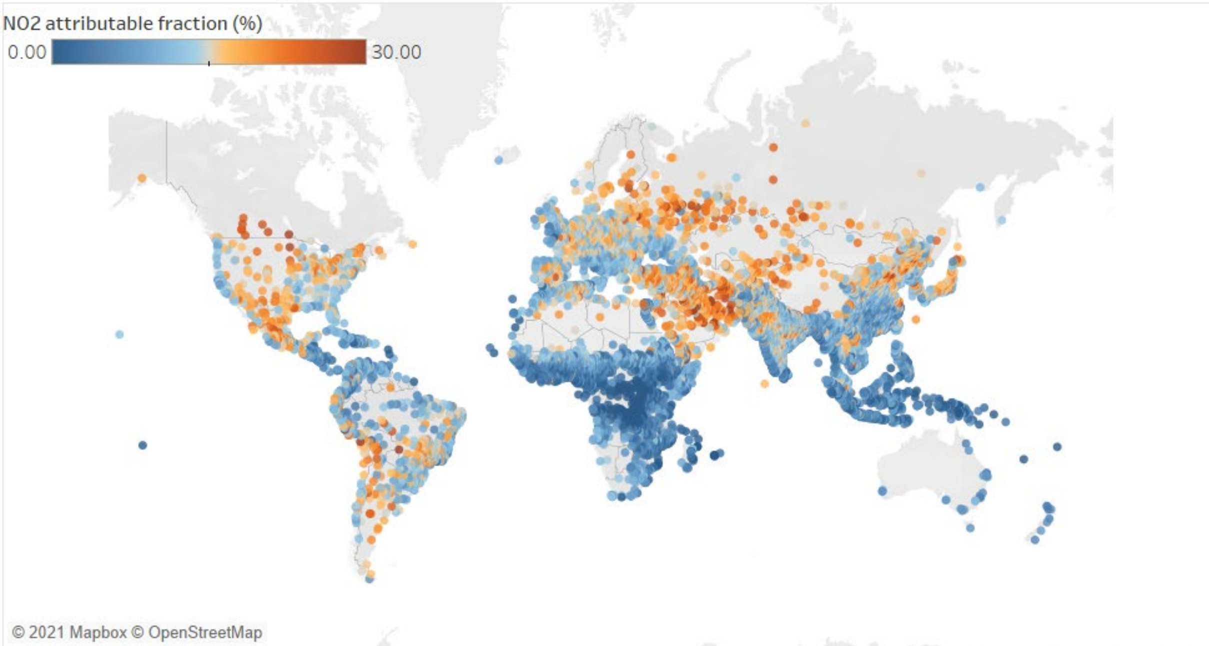

City Id	City Name	Sovereign	NO2 attributable fraction (%)
4355	Beirut	Lebanon	51.6
11392	Shenyang	China	35.1
12456	Shanghai	China	33.3
5703	Az Zubayr	Iraq	34.7
3686	Moscow	Russia	34.1
5767	Tehran	Iran	33.1
5451	Ad Diwaniyah	Iraq	33.6
4353	Saida	Lebanon	33.6
3407	Saint Petersburg	Russia	32.9
5908	Yazd	Iran	32.9

Figure S12. As for Figure S8, but for the fraction of pediatric asthma incidence attributable to NO_2 (%). Color bar saturates at 30% for greater contrast.

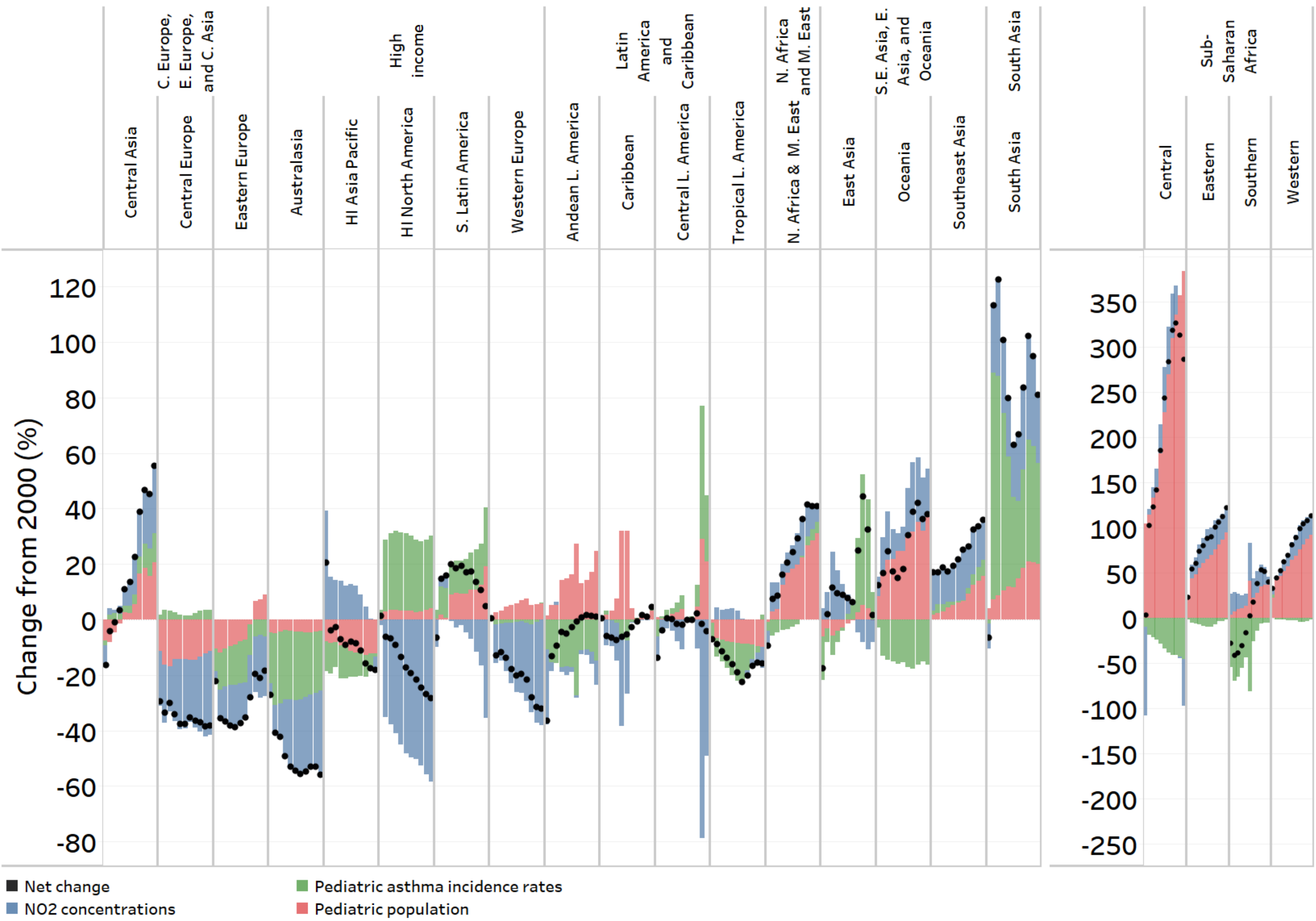

Figure S13. As for Figure 5, but for the change from 2000 to 2005 and 2010-2019 annually (represented left to right by the bars in each panel).

Supplemental References

(1) Lamsal, L. N.; Martin, R. V.; van Donkelaar, A.; Steinbacher, M.; Celarier, E. A.; Bucsela, E.; Dunlea, E. J.; Pinto, J. P. Ground-Level Nitrogen Dioxide Concentrations Inferred from the Satellite-Borne Ozone Monitoring Instrument. *J. Geophys. Res.* **2008**, *113* (D16). https://doi.org/10.1029/2007JD009235.

(2) Anenberg, S. C.; Henze, D. K.; Tinney, V.; Kinney, P. L.; Raich, W.; Fann, N.; Malley, C. S.; Roman, H.; Lamsal, L.; Duncan, B.; Martin, R. V.; van Donkelaar, A.; Brauer, M.; Doherty, R.; Jonson, J. E.; Davila, Y.; Sudo, K.; Kuylenstierna, J. C. I. Estimates of the Global Burden of Ambient PM2.5, Ozone, and NO2 on Asthma Incidence and Emergency Room Visits. *Environ. Health Perspect.* **2018**, *126* (10), 107004. https://doi.org/10.1289/EHP3766.

(3) Strode, S. A.; Ziemke, J. R.; Oman, L. D.; Lamsal, L. N.; Olsen, M. A.; Liu, J. Global Changes in the Diurnal Cycle of Surface Ozone. *Atmos. Environ.* **2019**, *199*, 323–333. https://doi.org/10.1016/j.atmosenv.2018.11.028.

(4) Orbe, C.; Oman, L. D.; Strahan, S. E.; Waugh, D. W.; Pawson, S.; Takacs, L. L.; Molod, A. M. Large-Scale Atmospheric Transport in GEOS Replay Simulations: TRANSPORT IN GEOS REPLAY SIMULATIONS. *J. Adv. Model. Earth Syst.* **2017**, *9* (7), 2545–2560. https://doi.org/10.1002/2017MS001053.

(5) Larkin, A.; Geddes, J. A.; Martin, R. V.; Xiao, Q.; Liu, Y.; Marshall, J. D.; Brauer, M.; Hystad, P. Global Land Use Regression Model for Nitrogen Dioxide Air Pollution. *Environ. Sci. Technol.* **2017**, *51* (12), 6957–6964. https://doi.org/10.1021/acs.est.7b01148.

(6) Gelaro, R.; McCarty, W.; Suárez, M. J.; Todling, R.; Molod, A.; Takacs, L.; Randles, C. A.; Darmenov, A.; Bosilovich, M. G.; Reichle, R.; Wargan, K.; Coy, L.; Cullather, R.; Draper, C.; Akella, S.; Buchard, V.; Conaty, A.; da Silva, A. M.; Gu, W.; Kim, G.-K.; Koster, R.; Lucchesi, R.; Merkova, D.; Nielsen, J. E.; Partyka, G.; Pawson, S.; Putman, W.; Rienecker, M.; Schubert, S. D.; Sienkiewicz, M.; Zhao, B. The Modern-Era Retrospective Analysis for Research and Applications, Version 2 (MERRA-2). *J. Clim.* **2017**, *30* (14), 5419–5454. https://doi.org/10.1175/JCLI-D-16-0758.1.

(7) Environment and Climate Change Canada/Environnement et Changement climatique Canada. National Air Pollution Surveillance Program https://open.canada.ca (accessed May 11, 2021).

(8) U.S. Environmental Protection Agency. Air Quality System Data Mart https://www.epa.gov/airdata (accessed Nov 24, 2020).

(9) European Environment Agency. Air Quality e-Reporting Air quality annual statistics https://www.eea.europa.eu/ (accessed May 11, 2021).

(10) Lamsal, L. N.; Duncan, B. N.; Yoshida, Y.; Krotkov, N. A.; Pickering, K. E.; Streets, D. G.; Lu, Z. U.S. NO2 Trends (2005–2013): EPA Air Quality System (AQS) Data versus Improved Observations from the Ozone Monitoring Instrument (OMI). *Atmos. Environ.* **2015**, *110*, 130–143. https://doi.org/10.1016/j.atmosenv.2015.03.055.

(11) Martin, R. V.; Brauer, M.; van Donkelaar, A.; Shaddick, G.; Narain, U.; Dey, S. No One Knows Which City Has the Highest Concentration of Fine Particulate Matter. *Atmospheric Environ. X* **2019**, *3*, 100040. https://doi.org/10.1016/j.aeaoa.2019.100040.